staining and Gallyas-Braak silver stain. For tau immunostaining, sections were immersed in 0.5% periodic acid for blocking intrinsic peroxidase and treated with 99% formic acid for 3 min. After blocking with 5% normal goat or horse serum, sections were incubated overnight with primary antibodies. The specific labeling was visualized using Vectastain Elite ABC kit (Vector, Burlingame, CA). Tissue sections were counterstained with hematoxylin. The following antibodies were used for immunostaining: tau154 (1:200), TAU-5 (1:1,000; Biosource. Camarillo, CA), AT8 (1:400; Innogenetics, Gent, Belgium; Murakami et al., 2006), antibodies to ApoD (1:1,000; Patel et al., 1995; 36C6, 1:100; Novocastra Laboratories, Newcastle, United Kingdom), antibodies to DCX (N-19, 1:200; C-18, 1:200; Santa Cruz Biotechnology, Santa Cruz, CA), antibody to Npas4 (1: 50, polyclonal antibody to purified Npas4; 1:100, NBP1-06574; Novus Biologicals, Littleton, CO), and antibody to Kcnab1 (1: 50; Santa Cruz Biotechnology).

Western Blotting

The remaining brain sample was homogenized in 9 volumes of Tris-saline buffer with protease inhibitors (Complete Inhibitor Cocktail tablets; Roche, Mannheim, Germany) and centrifuged at 55,000 rpm for 60 min at 4°C (TS buffer-soluble fraction). The pellet was homogenized again in 4 volumes of 1% sarkosyl in TS, incubated on ice for 30 min, and centrifuged at 55,000 rpm for 60 min at 4°C. The pellet was analyzed as the sarkosyl-insoluble fraction. The samples were boiled at 70°C in 4 volumes of SDS sample buffer, separated on 4–12% NuPAGE Bis-Tris Gel (Invitrogen, Carlsbad, CA), and the blots were labeled by antibodies. Signals were visualized with an enhanced chemiluminescence detection system (Pierce United Kingdom) and quantified by a luminoimage analyzer (LAS 1000-mini; Fuji Film, Tokyo, Japan). The signals were corrected by those of β-actin, and were tested for statistical significance using *t*-tests [TgTauP301L with NFTs and neuronal cell losses (n = 3) and without NFTs and neuronal cell losses (n = 3)]. All animal experiments were performed according to guidelines established in the *Guide for the care and use of laboratory animals* and by the ethical committee of Hirosaki University.

RESULTS

In comparing gene expression ratios between 517 and 512, 278 were increased and 162 were decreased. There were 477 increased gene expression ratios and 369 decreased gene expression ratios between 739 and 736. In the two comparisons of gene expression ratios, there were 52 up-regulations and 16 down-regulations in common. Among these 68 gene expressions, 37 gene expressions were significant, and 24 genes have already been described (Table I). There was no alteration of gene expression ratios for APP, MAPT, or GSK3β in 517, 512, 739, and 736 mouse brains.

According to biological pathways and gene expression groupings based on the GenMAPP database, comparison between 517 and 512 demonstrated seven down-regulated gene expression ratio groups. Five pathways consisted of up-regulated gene expression ratio groups. On comparison between 739 and 736, only one pathway showed a down-regulated gene expression group; however, 41 pathways showed up-regulated gene expression groups. Among these biological pathways, inflammatory response, mitochondrial fatty acid beta-oxidation, oxidative stress, apoptosis, and complement and coagulation cascades were commonly up-regulated.

To confirm further the differences in gene expression profile associated with NFT formation and neuronal cell losses, ApoD (Muffat and Walker, 2010), Npas4 (Lin et al., 2008), DCX (Moores et al., 2004), and Kcnab1 (Need et al., 2003) were selected for analysis at the protein level of up- or down-regulated genes among 24 significant genes because of the availability of antibodies. ApoD and DCX gene products had been previously suggested to be altered in AD (Thomas et al., 2003; Jin et al., 2004); however, others have not been reported.

On immunostaining, ApoD was markedly labeled in the brain of TgTauP301L with NFTs and neuronal cell losses compared with those of TgTauP301L without NFTs and neuronal cell losses. In particular, the hippocampus and white matter were markedly stained (Fig. 2b). Enhanced ApoD immunostaining was not detected in brains of TgTauP301L without NFTs and neuronal cell losses (Fig. 2a). The areas that exhibited extensive ApoD immunoreactivities were not related to those showing NFT formation and neuronal cell losses. Increased ApoD immunostaining was detected in neuronal processes, oligodendrocytes, and astrocytes (Fig. 2d) compared with that in 739 brains (Fig. 2c). Astrocytosis was also prominent in these areas. In AD and tauopathy brains, ApoD immunostaining was also detected mainly in astrocytes of the white matter and rarely in neurons in the cortex (Fig. 2f,g,i,j). ApoD was not detected in the control normal human brains (Fig. 2e,h).

Markedly decreased DCX immunoreactivities were observed in TgTauP301L showing NFTs and neuronal cell losses (Fig. 2l,n). Decrease in DCX-positive cells was observed even in areas without NFT formation. DCX-positive cells were detected in the dentate gyrus, hippocampus, and cerebral cortex of age-matched control nontransgenic mouse and TgTauP301L without NFTs and neuronal cell losses. Band-like immunoreactivities were prominent in the hippocampus of control age-matched nontransgenic mice (Fig. 2k,m). In AD and tauopathy brains, reticular immunoreactivity of DCX was markedly decreased in the dentate gyrus (Fig. 2p,q,s,t) compared with that in control human brains (Fig. 2o,r).

On Western blotting, the amount of DCX was decreased and the level of ApoD was increased in TgTauP301L mice with NFTs and neuronal cell losses compared with those in TgTauP301L without NFTs and neuronal cell losses (Fig. 3). The amounts of DCX and ApoD in sarkosyl-soluble fraction of the brain were correlated with the amount of sarkosyl-insoluble tau of the brain, suggesting that down-regulation of DCX and up-regulation of ApoD were closely associated with

TABLE I. Twenty-Four Up- and Down-Regulated Genes Shared in the Two Comparisons (517 vs. 512 and 739 vs. 736)

Description	Symbol	*P* value	Fold change (512/517)	Fold change (736/739)	Cell adhesion	Cell communication	Nervous system development	Development	Transport	Localization	DNA metabolism	Metabolism	Inflammatory response	Response to stimulus
Up-regulated														
Neuronal PAS domain protein 4	Npas4	0.03	2.33	2.77		*						*		
Thyrotropin releasing hormone	Trh	0.02	2.42	2.07		*								*
Immunoglobulin heavy chain 6 (heavy chain of IgM)	Igh-6	0.03	2.13	3.68		*			**	*		*		*
Syndecan 4	Sdc4	0.02	2.17	2.08										
Insulin receptor substrate 4	Irs4	0.02	2.11	2.10		*								
C-type lectin domain family 7, member a	Clec7a	0.04	2.21	6.62	**	*			**	*			**	*
Predicted gene 98	Gm98	0.02	3.50	2.90										
Holliday junction recognition protein	Hjurp	0.02	3.53	4.60										
Calcium/calmodulin-dependent protein kinase II inhibitor 1	Camk2n1	0.02	7.54	2.43										
Perilipin 4	Plin4	0.04	5.36	4.77										
Pyruvate dehydrogenase kinase, isoenzyme 4	Pdk4	0.03	2.80	2.28		*						*		
Proteasome (prosome, macropain) 26S subunit, ATPase 3, interacting protein	Psmc3ip	0.01	2.98	3.36							**	*		
Serine (or cysteine) peptidase inhibitor, clade A, member 3N	Serpina3n	0.02	2.65	5.47										*
Apolipoprotein D	Apod	0.03	2.05	3.55					**	*				
Periostin, osteoblast specific factor	Postn	0.02	2.01	2.23	**	*		*						
Carboxypeptidase M	Cpm	0.02	2.08	2.18								*		
Myelin-associated oligodendrocytic basic protein	Mobp	0.02	2.08	2.00										
Down-regulated														
Membrane protein, palmitoylated 4 (MAGUK p55 subfamily member 4)	Mpp4	0.01	0.40	0.29										
Pituitary tumor-transforming gene 1	Pttg1	0.00	0.09	0.11							**	*		*
Doublecortin	Dcx	0.01	0.39	0.32		*	**	*		*				
Potassium voltage-gated channel, shaker-related subfamily, beta member 1	Kcnab1	0.02	0.40	0.47					**	*				
RNA binding motif protein 45	Rbm45	0.00	0.27	0.26			**	*						
Succinate dehydrogenase complex, subunit A, flavoprotein (Fp)	Sdha	0.01	0.36	0.16					**	*		*		
RIKEN cDNA 4933400F03 gene	4933400 F03Rik	0.02	0.50	0.50										

*$P < 0.05$.
**$P < 0.01$.

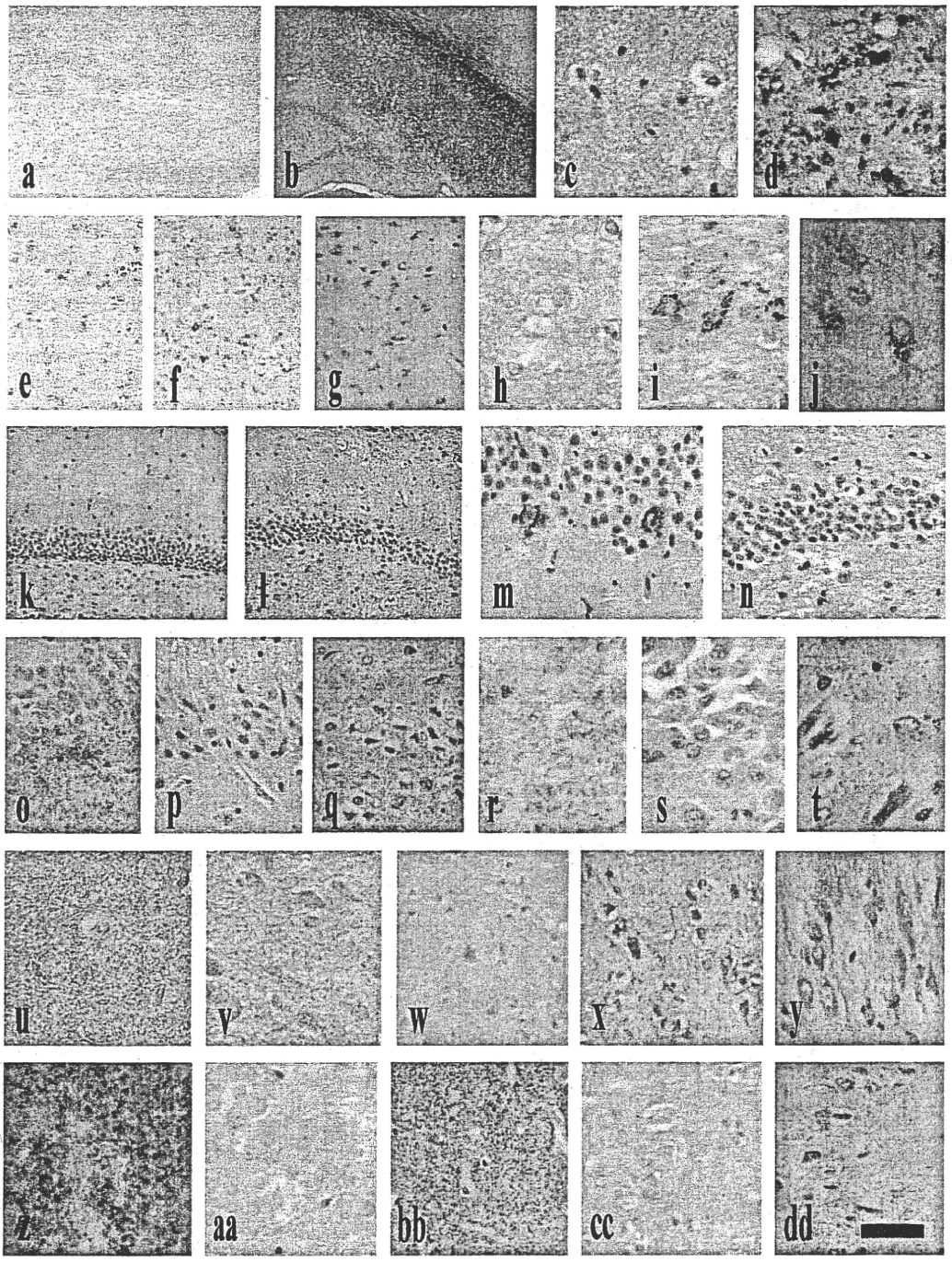

Fig. 2. Immunostaining of ApoD, DCX, Npas4, and Kcnab1. Staining of ApoD (from Patel; **a–d**), ApoD(36C6) (**e–j**), DCX (N19; **k–t**), Npas4 (polyclonal; **u–y**), and Kcnab1 (**z–dd**) in TgTauP301L without NFTs and neuronal cell losses (a,c,k,m,u,z), with NFTs and neuronal cell losses (b,d,l,n,v,aa), control human brains (e,h,o,r,w,bb), AD brains (f,i,p,s,x,cc), and FTD brains (g,j,q,t,y,dd). Staining of ApoD and Npas4 was increased in TgTauP301L brain with NFTs and neuronal cell losses, AD brains, and FTD brains compared with that in TgTauP301L brain without NFTs and neuronal cell losses and control brain. Decreased immunoreactivities of DCX and Kcnab1 were recognized in TgTauP301L brain with NFTs and neuronal cell losses, AD brain, and FTD brains. Scale bar = 50 μm in dd (applies to e–g,m–q,w–y,bb–dd); 250 μm for a,b; 100 μm for c,d,k,l; 25 μm for h–j,r–v,z,aa. [Color figure can be viewed in the online issue, which is available at wileyonlinelibrary.com.]

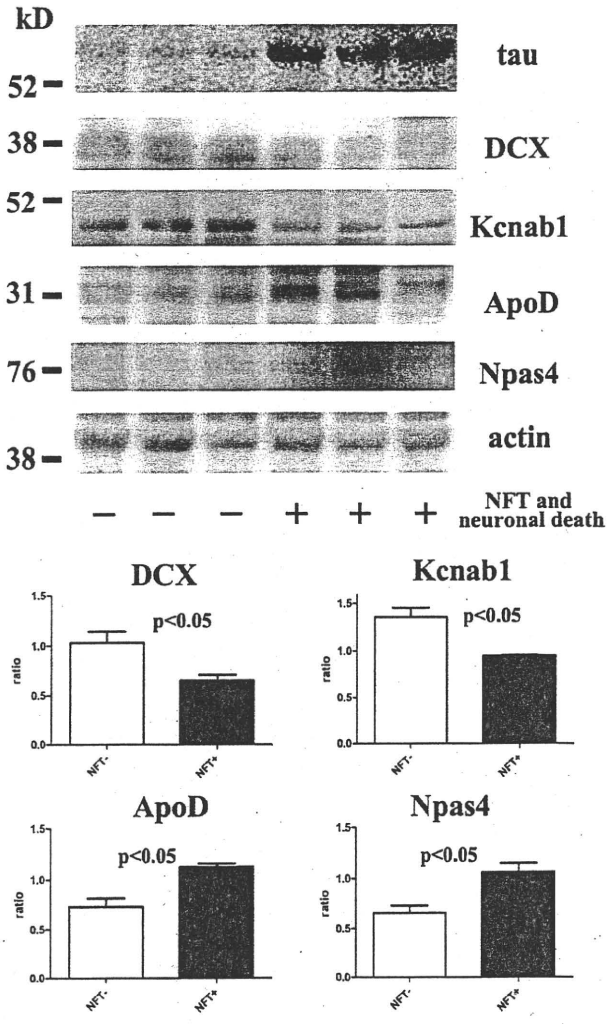

Fig. 3. Western blotting of brain extracts using tau (TAU-5), DCX (C-18), Kcnab1, ApoD, and Npas4 antibodies. Insoluble tau accumulation (TAU-5) was correlated with decreased levels of DCX (C18) and Kcnab1 and increased levels of ApoD (from Patel) and Npas4 (NBP1-06574). Plus signs indicate brain extracts of TgTauP301L with NFTs and neuronal cell losses, and minus signs indicate those of TgTauP301L without NFTs and neuronal cell losses. The signals were corrected by those of β-actin and were tested for statistical significance by using *t*-test.

NFT formation and neuronal cell losses at the gene product level (Fig. 3).

Immunostaining of Npas4 was increased in cerebral cortex and hippocampus of TgTauP301L brains with NFTs and neuronal losses (Fig. 2v) and also in AD and tauopathy brains (Fig. 2x,y). Immunoreactivity of Kcnab1 was decreased in cortex and hippocampus of TgTauP301L brains with NFTs and neuronal losses (Fig. 2aa) and also in AD and tauopathy brains (Fig. 2cc,dd). On Western blotting, the amount of Npas4 was increased and the level of Kcnab1 was decreased in TgTauP301L mice with NFTs and neuronal cell losses compared with those in TgTauP301L without NFTs and neuronal cell losses (Fig. 3). Therefore, changed expression level of Npas4 and Kcnab1 was also verified at the protein level.

DISCUSSION

Our oligonucleotide array expression study demonstrated that gene expression groups were altered in many biological pathways and that these collective alterations were closely related to the final stage of tauopathy, namely, NFT formation and neuronal cell losses. Both sets of comparisons of mice with or without NFTs and neuronal cell losses showed that five pathways including oxidative stress, apoptosis, mitochondrial fatty acid betaoxidation, inflammatory response, and complement and coagulation cascades are consistently up-regulated, suggesting that NFTs and neuronal losses occurred on the basis of at least these enhanced biological pathways with many up-regulated gene cluster expressions. Then, altered gene expression ratios demonstrated in both comparison sets consisting of 17 up-regulated genes and seven down-regulated genes and biological processes were summarized by Gene Ontology (Table I). Reported roles of up-regulated genes were classified into inhibitory synapse development (Npas4), metabolism (thyrotropin-releasing hormone, insulin receptor substrate 4, pyruvate dehydrogenase kinase, isoenzyme 4), inflammation [immunoglobulin heavy chain 6, C-type lectin domain family 7, member a, serine (or cysteine) peptidase inhibitor, clade A, member 3N, carboxypeptidase M], brain development (syndecan 4), CNS myelination (predicted gene 98, myelin-associated oligodendrocytic basic protein), cell cycle regulation (Holliday junction recognition protein), protein kinase or phosphatase activity (calcium/calmodulin-dependent protein kinase II inhibitor 1), body weight regulation (perilipin 4), proteosome system [proteasome (prosome, macropain) 26S subunit, ATPase 3, interacting protein], lipid transportation (ApoD), and tumorigenesis (periostin, osteoblast specific factor). These findings indicated that NFT formation and neuronal cell losses were associated with up-regulated conditions of CNS regeneration, metabolism, lipid transportation, proteosome function, cell cycle regulation and signaling, and inflammation. Down-regulated genes were classified into photoreceptor synaptic calcium handling (membrane protein, palmitoylated 4), neuronal protection (pituitary tumor-transforming gene 1), neurogenesis (DXC), synaptic plasticity and learning (Kcnab1), mitochondrial function (succinate dehydrogenase complex, subunit A, flavoprotein), and others (RNA binding motif protein 45, RIKEN cDNA 4933400F03 gene). These conditions can also be summarized as suppressed neuronal and synaptic function, neurogenesis, and mitochondrial dysfunction.

Among these NFTs and neuronal cell loss-related gene expressions, ApoD has been reported to be elevated in the brains and cerebrospinal fluid of AD patients

(Terrisse et al., 1998; Kalman et al., 2000). ApoD is detected in oligodendrocytes, astrocytes, neurons with NFTs, and the vicinity of senile plaques, and the level of ApoD is associated with the severity of NFTs, but not that of Aβ (Belloir et al., 2001; Glöckner and Ohm, 2003). Accumulation of ApoD has been reported in another tauopathy, Nieman Pick type C brains (Ong et al., 2002). ApoD rapidly increases with various types of brain damage and peripheral nerve regeneration (Boyles et al., 1990) and is involved in the mechanisms regulating protection from oxidative stress (Andersen, 2004; Ganfornina et al., 2008). In our study, the level of ApoD was prominently increased in the brains of mice with NFTs and neuronal cell losses as well as gene expressions. Because our mice and Nieman Pick type C patients exhibit tauopathy findings without Aβ, the increased level of ApoD appears closely related to NFT formation and neuronal cell losses. NFT-mediated neurotoxicity and increased oxidative stress may increase the level of ApoD.

We also found that the expression of DCX gene and the amount of DCX were decreased in brains with NFTs and neuronal cell losses. The level of DCX is inversely correlated with accumulation of insoluble tau aggregation. DCX is one of the microtubule-binding proteins for axonal growth and collateral branching and essential in postmitotic neurons for brain development (Moores et al., 2004; Tint et al., 2009), indicating that DCX is a marker of neurogenesis. Although a first report suggested an increased amount of DCX accompanying hippocampal neurogenesis in AD brains (Jin et al., 2004), others did not show consistent results (Boekhoorn et al., 2006a; Verwer et al., 2007). Aβ decreases the DCX-positive cells in the hippocampus in APP model mice (Zhang et al., 2007; Mirochnic et al., 2009). In tau transgenic mouse models, however, DCX-positive neurogenesis was increased in an early phase (Boekhoorn et al., 2006b; Schindowski et al., 2008). In the late stage with NFT formation, up-regulation of cell cycle events and decreased DCX levels occurred, accompanied by neuronal cell losses (Schindowski et al., 2008). These findings corresponded to our findings and suggest that suppressed neurogenesis is one of the causal factors underlying neuronal cell losses in brains with tauopathy.

Npas4 is a newly identified transcription factor that plays a role in the development of inhibitory synapses (Lin et al., 2008) and stress-induced impairment of hippocampal function (Yun et al., 2010). Kcnab1 is also associated with excitability in hippocampal neurons and impairment of learning and memory (Need et al., 2003). Altered gene expressions of both hippocampal proteins were confirmed at protein levels. Although roles of Npas4 and Kcnb1 have not been precisely clarified, our findings suggest that these novel molecules participate in cascades from tau accumulation to NFT formation and neuronal cell losses leading to memory disturbance. Thus, gene expression profile and confirmations at protein level are useful methods for clarifying the constituent molecules of tauopathy.

Recent studies in an NFT mouse model showed that NFTs are neurotoxic and cause delayed neuronal cell losses without the usual caspase-dependent apoptosis leading to acute neuronal cell losses (Spires-Jones et al., 2008; de Calignon et al., 2009). Age-dependent reinforcement of tau accumulation and mitochondrial dysfunction-related energy metabolism and oxidative stress leads to NFTs and apoptotic neuronal cell losses (Kulic et al., 2010). Given these findings, neuronal cell losses may be caused by NFT neurotoxicity, suppressed neurogenesis, and apoptosis accompanying NFT formation induced by many biological pathways. To develop therapy for neuronal cell losses as a final target of tauopathy, every step of these biological pathways and key molecules must be clarified.

ACKNOWLEDGMENTS

We thank K. Sato, M. Ono, K. Iinuma, Y. Sato, R. Tsushima, and I. Shirahama for technical assistance; Dr. Koichi Ishiguro for tau154; and Dr. Shutish C. Patel for anti-ApoD antibody.

REFERENCES

Andersen JK. 2004. Oxidative stress in neurodegeneration: cause or consequence? Nat Med 10:S18–S25.

Belloir B, Kövari E, Surini-Demiri M, Savioz A. 2001. Altered apolipoprotein D expression in the brain of patients with Alzheimer disease. J Neurosci Res 64:61–69.

Benjamini Y, Hochberg Y. 1995. Controlling the false discovery rate: a practical and powerful approach to multiple testing. J R Statist Soc B 57:289–300.

Boekhoorn K, Joels M, Lucassen PJ. 2006a. Increased proliferation reflects glial and vascular-associated changes, but not neurogenesis in the presenile Alzheimer hippocampus. Neurobiol Dis 24:1–14.

Boekhoorn K, Terwel D, Biemans B, Borghgraef P, Wiegert O, Ramakers GJ, de Vos K, Krugers H, Tomiyama T, Mori H, Joels M, van Leuven F, Lucassen PJ. 2006b. Improved long-term potentiation and memory in young tau-P301L transgenic mice before onset of hyperphosphorylation and tauopathy. J Neurosci 26:3514–3523.

Boyles JK, Notterpek LM, Anderson LJ. 1990. Accumulation of apolipoproteins in the regenerating and remyelinating mammalian peripheral nerve. Identification of apolipoprotein D, apolipoprotein A-IV, apolipoprotein E, and apolipoprotein A-I. J Biol Chem 265:17805–17815.

de Calignon A, Spires-Jones TL, Pitstick R, Carlson GA, Hyman BT. 2009. Tangle-bearing neurons survive despite disruption of membrane integrity in a mouse model of tauopathy. J Neuropathol Exp Neurol 68:757–761.

Ganfornina MD, Do Carmo S, Lora JM, Torres-Schumann S, Vogel M, Allhorn M, González C, Bastiani MJ, Rassart E, Sanchez D. 2008. Apolipoprotein D is involved in the mechanisms regulating protection from oxidative stress. Aging Cell 7:506–515.

Glöckner F, Ohm TG. 2003. Hippocampal apolipoprotein D level depends on Braak stage and APOE genotype. Neuroscience 22:103–110.

Hardy J. 2009. The amyloid hypothesis for Alzheimer's disease: a critical reappraisal. J Neurochem 110:1129–1134.

Holmes C, Boche D, Wilkinson D, Yadegarfar G, Hopkins V, Bayer A, Jones RW, Bullock R, Love S, Neal JW, Zotova E, Nicoll JA. 2008. Long-term effects of Aβ42 immunization in Alzheimer's disease: follow-up of a randomised, placebo-controlled phase I trial. Lancet 372:216–223.

Jin K, Peel AL, Mao XO, Xie L, Cottrell BA, Henshall DC, Greenberg DA. 2004. Increased hippocampal neurogenesis in Alzheimer's disease. Proc Natl Acad Sci U S A 101:343–347.

Kalman J, McConathy W, Araoz C, Kasa P, Lacko AG. 2000. Apolipoprotein D in the aging brain and in Alzheimer's dementia. Neurol Res 22:330–336.

Kim SY, Volsky DJ. 2005. PAGE: parametric analysis of gene set enrichment. BMC Bioinformatics 6:144.

Kulic L, Wollmer MA, Rhein V, Pagani L, Kuehnle K, Cattepoel S, Tracy J, Eckert A, Nitsch RM. 2010. Combined expression of tau and the Harlequin mouse mutation leads to increased mitochondrial dysfunction, tau pathology and neurodegeneration. Neurobiol Aging [E-pub ahead of print].

Lin Y, Bloodgood BL, Hauser JL, Lapan AD, Koon AC, Kim TK, Hu LS, Malik AN, Greenberg ME. 2008. Activity-dependent regulation of inhibitory synapse development by Npas4. Nature 455:1198–1204.

Mirochnic S, Wolf S, Staufenbiel M, Kempermann G. 2009. Age effects on the regulation of adult hippocampal neurogenesis by physical activity and environmental enrichment in the APP23 mouse model of Alzheimer disease. Hippocampus 19:1008–1018.

Moores CA, Perderiset M, Francis F, Chelly J, Houdusse A, Milligan RA. 2004. Mechanism of microtubule stabilization by doublecortin. Mol Cell 14:833–839.

Muffat J, Walker DW. 2010. Apolipoprotein D: an overview of its role in aging and age-related diseases. Cell Cycle 9:269–273.

Murakami T, Paitel E, Kawarabayashi T, Ikeda M, Chishti MA, Janus C, Matsubara E, Sasaki A, Kawarai T, Phinney AL, Harigaya Y, Horne P, Egashira N, Mishima K, Hanna A, Yang J, Iwasaki K, Takahashi M, Fujiwara M, Ishiguro K, Bergeron C, Carlson GA, Abe K, Westaway D, St. George-Hyslop P, Shoji M. 2006. Cortical neuronal and glial pathology in TgTauP301L transgenic mice: neuronal degeneration, memory disturbance, and phenotypic variation. Am J Pathol 169:1365–1375.

Need AC, Irvine EE, Giese KP. 2003. Learning and memory impairments in $K_v\beta1.1$-null mutants are rescued by environmental enrichment or ageing. Eur J Neurosci 18:1640–1644.

Ong WY, Hu CY, Patel SC. 2002. Apolipoprotein D in the Niemann-Pick type C disease mouse brain: an ultrastructural immunocytochemical analysis. J Neurocytol 31:121–129.

Paquet D, Bhat R, Sydow A, Mandelkow EM, Berg S, Hellberg S, Fälting J, Distel M, Köster RW, Schmid B, Haass C. 2009. A zebrafish model of tauopathy allows in vivo imaging of neuronal cell death and drug evaluation. J Clin Invest 119:1382–1395.

Patel SC, Asotra K, Patel YC, McConathy WJ, Patel RC, Suresh S. 1995. Astrocytes synthesize and secrete the lipophilic ligand carrier apolipoprotein D. Neuroreport 6:653–657.

Santacruz K, Lewis J, Spires T, Paulson J, Kotilinek L, Ingelsson M, Guimaraes A, DeTure M, Ramsden M, McGowan E, Forster C, Yue M, Orne J, Janus C, Mariash A, Kuskowski M, Hyman B, Hutton M, Ashe KH. 2005. Tau suppression in a neurodegenerative mouse model improves memory function. Science 309:476–481.

Schindowski K, Belarbi K, Bretteville A, Ando K, Buée L. 2008. Neurogenesis and cell cycle-reactivated neuronal death during pathogenic tau aggregation. Genes Brain Behav 7:92–100.

Smyth GK. 2004. Linear models and empirical bayes methods for assessing differential expression in microarray experiments. Stat Appl Genet Mol Biol 3:Article 3.

Spires-Jones TL, de Calignon A, Matsui T, Zehr C, Pitstick R, Wu HY, Osetek JD, Jones PB, Bacskai BJ, Feany MB, Carlson GA, Ashe KH, Lewis J, Hyman BT. 2008. In vivo imaging reveals dissociation between caspase activation and acute neuronal death in tangle-bearing neurons. J Neurosci 28:862–867.

Spires-Jones TL, Stoothoff WH, de Calignon A, Jones PB, Hyman BT. 2009. Tau pathophysiology in neurodegeneration: a tangled issue. Trends Neurosci 32:150–159.

Stokin GB, Lillo C, Falzone TL, Brusch RG, Rockenstein E, Mount SL, Raman R, Davies P, Masliah E, Williams DS, Goldstein LS. 2005. Axonopathy and transport deficits early in the pathogenesis of Alzheimer's disease. Science 307:1282–1288.

Terrisse L, Poirier J, Bertrand P, Merched A, Visvikis S, Siest G, Milne R, Rassart E. 1998. Increased levels of apolipoprotein D in cerebrospinal fluid and hippocampus of Alzheimer's patients. J Neurochem 71:1643–1650.

Thomas EA, Laws SM, Sutcliffe JG, Harper C, Dean B, McClean C, Masters C, Lautenschlager N, Gandy SE, Martins RN. 2003. Apolipoprotein D levels are elevated in prefrontal cortex of subjects with Alzheimer's disease: no relation to apolipoprotein E expression or genotype. Biol Psychiatry 54:136–141.

Tint I, Jean D, Baas PW, Black MM. 2009. Doublecortin associates with microtubules preferentially in regions of the axon displaying actin-rich protrusive structures. J Neurosci 29:10995–11010.

Verwer RW, Sluiter AA, Balesar RA, Baayen JC, Noske DP, Dirven CM, Wouda J, van Dam AM, Lucassen PJ, Swaab DF. 2007. Mature astrocytes in the adult human neocortex express the early neuronal marker doublecortin. Brain 130:3321–3335.

Yun J, Koike H, Ibi D, Toth E, Mizoguchi H, Nitta A, Yoneyama M, Ogita K, Yoneda Y, Nabeshima T, Nagai T, Yamada K. 2010. Chronic restraint stress impairs neurogenesis and hippocampus-dependent fear memory in mice: possible involvement of a brain-specific transcription factor Npas4. J Neurochem 114:1840–1851.

Zhang C, McNeil E, Dressler L, Siman R. 2007. Long-lasting impairment in hippocampal neurogenesis associated with amyloid deposition in a knock-in mouse model of familial Alzheimer's disease. Exp Neurol 204:77–87.

Journal of Neuroscience Research

Journal of Neuroscience Research 88:3547–3554 (2010)

Amyloid β Accelerates Phosphorylation of Tau and Neurofibrillary Tangle Formation in an Amyloid Precursor Protein and Tau Double-Transgenic Mouse Model

Yusuke Seino,[1] Takeshi Kawarabayashi,[2*] Yasuhito Wakasaya,[2] Mitsunori Watanabe,[2] Ayumi Takamura,[2] Yukiko Yamamoto-Watanabe,[2] Tomoko Kurata,[3] Koji Abe,[3] Masaki Ikeda,[4] David Westaway,[5] Tetsuro Murakami,[6] Peter St. George Hyslop,[6] Etsuro Matsubara,[2] and Mikio Shoji[2]

[1]Department of General Medicine, Mutsu General Hospital, Mutsu, Japan
[2]Department of Neurology, Hirosaki University Graduate School of Medicine, Hirosaki, Japan
[3]Department of Neurology, Okayama University Graduate School of Medicine and Dentistry, Okayama, Japan
[4]Department of Neurology, Gunma University Graduate School of Medicine, Maebashi, Japan
[5]Centre for Prions and Protein Folding Diseases, University of Alberta, Edmonton, Alberta, Canada
[6]Canada Centre for Research in Neurodegenerative Diseases, University of Toronto, Toronto, Ontario, Canada

In Alzheimer's disease, Aβ deposits are considered the initial cardinal events that induce tauopathy secondarily. However, the relationship between Aβ amyloidosis and tauopathy has not been determined in detail. We produced double transgenic mice, $2\times TgTau^{+/-}APP^{+/-}$, by mating Tg2576 mice that exhibit Aβ amyloidosis and TgTauP301L mice that show tauopathy, and statistically analyzed the effect of Aβ accumulation on tauopathy. There was no significant difference in the progression of Aβ accumulation among $2\times TgTau^{+/-}APP^{+/-}$ and $1\times TgTau^{-/-}APP^{+/-}$, and tau accumulation among $2\times TgTau^{+/-}APP^{+/-}$ and $1\times TgTau^{+/-}APP^{-/-}$. The appearance rates of phosphorylated tau developing in neurons and processes were significantly accelerated in $2\times TgTau^{+/-}APP^{+/-}$ mice compared with those in $1\times TgTau^{+/-}APP^{-/-}$ mice at 23 months of age. Accumulation of phosphorylated and confomationally altered tau and GSK3β in neuronal processes was accelerated in the white matter in $2\times TgTau^{+/-}APP^{+/-}$. The level of phosphorylated tau in the sarkosyl-insoluble fraction was increased in $2\times TgTau^{+/-}APP^{+/-}$ brains compared with that in $1\times TgTau^{+/-}APP^{-/-}$ brains. Thus, Aβ amyloid partially enhances tauopathy through accumulation of insoluble, phosphorylated, and conformationally changed tau in neuronal cytoplasm and processes in the late stage.

Key words: Alzheimer's disease; double transgenic mouse; neurofibrillary tangles

Alzheimer's disease (AD) brains are invariably characterized by two pathological features, initial Aβ amyloidosis by extracellular deposition of Aβ and subsequent intracellular accumulation of neurofibrillary tangles (NFTs) comprising abnormal aggregates of phosphorylated tau. Aβ cascade from Aβ deposits to the final appearance of tauopathy and neuronal cell losses is the major hypothesis that explains all steps in the pathogenesis of AD. Soluble Aβ oligomers are considered the cardinal molecules that adversely affect synaptic structures and plasticity (Hardy, 2009). Tauopathy is present in sporadic frontotemporal dementia such as progressive supranuclear palsy and corticobasal degeneration and caused by MAPT gene mutation itself in FTDP-17 (Hutton et al., 1998). Other types of diseases such as brain amyloids of familial British dementia (Ghiso et al., 2001) and lysosomal disorders of Niemann-Pick disease type C also induce numerous NFTs (Love et al., 1995). Because JNPL3 mice expressing double APP and tau mutations exhibited substantial enhanced NFT pathology in the limbic system and

Contract grant sponsor: Ministry of Health, Labor and Welfare of Japan; Contract grant number: 19390233 (to M.S.); Contract grant number: 19590976 (to T.Ka.); Contract grant number: 18590968 (to E.M.); Contract grant sponsor: Ministry of Education, Culture, Sports, Science and Technology, Japan (to M.S.); Contract grant sponsor: The Mochida Memorial Foundation for Medical and Pharmaceutical Research (to M.W.); Contract grant sponsor: Hirosaki University Institutional Research (to M.S.).

*Correspondence to: Takeshi Kawarabayashi, Department of Neurology, Institute of Brain Science, Hirosaki University Graduate School of Medicine 5 Zaifucho, Hirosaki 036-8562, Japan.
E-mail: tkawara@cc.hirosaki-u.ac.jp

Received 12 May 2010; Revised 5 August 2010; Accepted 17 August 2010

Published online 8 October 2010 in Wiley Online Library (wileyonlinelibrary.com). DOI: 10.1002/jnr.22516

olfactory cortex (Lewis et al., 2001), investigations into mechanisms underlying Aβ induced tauopathy have been facilitated. Accumulation of phosphorylated tau was enhanced around senile plaque cores (Tomidokoro et al., 2001). Injection of Aβ42 fibrils or brain Aβ extracts into the brains of the tau transgenic mice models caused increases in the number of NFTs (Götz et al., 2001). Administration of Aβ antibodies cleared Aβ deposits and delayed subsequent tauopathy in a 3×Tg-AD mouse model (Oddo et al., 2004). Blocking Aβ42 or Aβ oligomer accumulation delayed the onset and progression of tau pathology (Oddo et al., 2008). Reduction of both soluble Aβ and tau levels have been suggested as necessary to rescue cognitive impairment in 3×Tg-AD model mice (Oddo et al., 2006a). In contrast, augmenting tau levels did not modulate the onset or progression of Aβ pathology (Oddo et al., 2007). Thus, a unidirectional mechanism from Aβ amyloids to tauopathy is suggested in transgenic mouse models. However, follow-up of a phase I trial of immunization with Aβ42 did not prevent clinical progression of dementia, tauopathy, or neuronal cell loss, even though it resulted in the clearance of amyloid plaques (Holmes et al., 2008). These findings have facilitated further clarification of the precise mechanisms underlying induction of tauopathy by Aβ amyloidosis.

We have established a tauopathy model mouse expressing 2N4R human tauP301L (TgTauP301L), which develops a florid pathology that includes numerous pretangles, NFTs, and glial fibrillary tangles (GFTs) in the frontotemporal areas of the cerebrum, accompanied by gliosis, neuronal loss, and cerebral atrophy. Accumulated tau was hyperphosphorylated, conformationally changed, ubiquitinated, and sarkosyl insoluble. These mice exhibited impairment in hippocampus-dependent and -independent behavioral paradigms and showed substantial phenotypic variation and a spectrum of pathologies similar to that observed in FTDP-17 patients (Murakami et al., 2006). Here, we generated double transgenic mice, $2\times TgTau^{+/-}APP^{+/-}$, by mating Tg2576 mice that exhibit marked Aβ deposits (Kawarabayashi et al., 2004) with TgTauP301L mice in order to analyze how Aβ amyloids induces tauopathy. Progression of deposits of Aβ, phosphorylated and conformatinally changed tau, NFTs, GFT, and phenotypic variation were compared among $2\times TgTau^{+/-}APP^{+/-}$, $1\times Tau^{+/-}APP^{-/-}$, $1\times TgTau^{-/-}APP^{+/-}$, and $0\times TgTau^{-/-}APP^{-/-}$ mice. Although there were no significant changes in the progression of Aβ and tau deposits from 8 to 16 months of age, the presence of phosphorylated and conformationally changed tau in dystrophic neurites around senile plaques and neuropil threads and the appearance of pretangles and NFTs were significantly enhanced in $2\times TgTau^{+/-}APP^{+/-}$ at 23 months of age. Based on these findings, the acceleration of tauopathy by Aβ amyloidosis was considered slow and not very strong, requiring a long incubation period during which phosphorylation, conformational change, and insolubilization of tau occurred.

MATERIALS AND METHODS

Transgenic Mouse Models

To generate double transgenic mice expressing tauP301L and βAPP KM670/671NL, TgTauP301L maintained in the FVB/N strain were mated with Tg2576 mice maintained in the B6/SJL strain and defined as $2\times TgAPP^{+/-}Tau^{+/-}$. Heterozygote F1 littermates of TgTauP301 and Tg2576 were used for all experiments to analyze uniform genetic background mice as FVB/B6/SJL. Each genotypic strain was $2\times TgTau^{+/-}APP^{+/-}$ expressing human 2N4R tauP301L and βAPP KM670/671NL, $1\times TgTau^{+/-}APP^{-/-}$, $1\times TgTau^{-/-}APP^{+/-}$, and $0\times Tg Tau^{-/-}APP^{-/-}$, which was the wild FVB/B6/SJL mouse expressing only endogenous mouse APP and tau. In total 124 mice were examined. Twenty-three $2\times TgTau^{+/-}APP^{+/-}$ (3 mice at 8 months of age, 4 mice at 12 months, 6 mice at 16 months, and 8 mice at 23 months), 62 $1\times TgTau^{+/-}APP^{-/-}$ (7 mice at 8 months, 15 mice at 12 months, 27 mice at 16 months, and 13 mice at 23months), 16 $1\times TgTau^{-/-}APP^{+/-}$ (1 mouse at 8 months, 1 mouse at 12 months, 5 mice at 16 months, and 9 mice at 23 months), and 23 $0\times TgTau^{-/-}APP^{-/-}$ (16 mice at 8 months, 1 mouse at 12 months, 19 mice at 16 months, and 4 mice at 23 months) were analyzed. All animal experiments were performed according to guidelines established in the Guide for the care and use of laboratory animals and the ethical committee of Hirosaki University.

Immunostaining

After mice were sacrificed under ether anesthesia, brains were removed and cut sagitally along the midline. One hemisphere was fixed in 4% paraformaldehyde with 0.1 M phosphate buffer (pH 7.6) for 8 hr and embedded in paraffin. Five-micrometer-thick sections were prepared for immunostaining and Gallyas-Braak silver stain. Sections were immersed in 0.5% periodic acid to block intrinsic peroxidase and treated with 99% formic acid for 3 min. Microwave pretreatment was used for AT8 staining. After blocking with 5% normal goat or horse serum in 50 mM phosphate-buffered saline (pH 7.4) containing 0.05% Tween 20 and 4% Block Ace (Snow Brand, Sapporo, Japan), sections were incubated overnight with primary antibodies. Specific labeling was visualized by Vectastain Elite ABC kit (Vector, Burlingame, CA). Tissue sections were counterstained with hematoxylin. The following antibodies were used in this study: tau-154, against amino acids 154–168 of human tau441 that specifically detect human tau (1:200); HT7. against amino acids 159–163 of human tau441 that specifically detect human tau (1:500; Innogenetics, Gent, Belgium); CP27, against all forms of human tau (1:500); TAU-5, against amino acids of human tau441 that detects both human and mouse tau (1:1,000; Abcam, Cambridge, MA); MC1, against early epitope of confomationally changed tau (1:400); PS199, against phosphorylated tau at serine199 (1:500); CP13, against phosphorylated tau at serine202 (1:400); AT8, against phosphorylated tau at serine202/threonine205 (1:400; Innogenetics); anti-PT231/PS235, against phosphorylated tau at threonine231/serine235 (1:500); PHF-1, against phosphorylated tau at serine396/serine404 (1:400); anti-PS413, against phosphorylated tau at serine413 (1:100);

Ab9204, against N-terminal aspartate of Aβ (0.1 μg/ml); and anti-GSK3β antibody (1:100) were used (Tomidokoro et al., 2001).

Western Blot

The other half of the mouse brain was weighed and homogenized using a motor-driven Teflon glass homogenizer for 20 strokes in 9 volumes of Tris-saline buffer (TS) with protease inhibitors (TS inhibitors 50 mM Tris-HCl and 150 mM NaCl, pH 7.6, with protease inhibitor cocktail; Complete; Roche Diagnostics, Indianapolis, IN). The homogenate was centrifuged at 55,000 rpm for 60 min at 4°C, and the supernatant was analyzed as the TS-soluble fraction. After washing with 10 volumes of TS with protease inhibitors, the pellet was homogenized again in 4 volumes of 1% sarkosyl in TS inhibitors, incubated on ice for 30 min, and centrifuged at 55,000 rpm for 60 min at 4°C. The supernatant was analyzed as the sarkosyl-soluble fraction. The pellet was washed twice with 10 volumes of 1% sarkosyl in TS inhibitors, and the remaining pellet was analyzed as the sarkosyl-insoluble fraction. Each sample was boiled at 70°C in SDS sample buffer, separated on 4–12% NuPAGE Bis-Tris Gel (Invitrogen, Carlsbad, CA), and electrotransferred to Immobilon P (Millipore, Bedford, MA) at 100 V for 1.5 hr. The blots were labeled by HT-7, Tau5, PHF-1, AT8, and CP13. The signal intensity of labeled protein using Supersignal (Pierce, Rockford, IL) was quantified by the luminoimage analyzer (LAS 1000-Mini; Fuji Film, Tokyo, Japan).

RESULTS

Appearance of expressed human tauP301L began at 3 months of age in both $2\times TgTau^{+/-}APP^{+/-}$ and $1\times TgTau^{+/-}APP^{-/-}$. With aging, the human tauP301L accumulated progressively and distributed widely from the hippocampus to the cerebral cortices, thalamus, amygdale, striatum, and brainstem. There were no significant differences observed in initiation, distribution, and progression of human tauP301L accumulation between $2\times TgTau^{+/-}APP^{+/-}$ (Fig. 1a–d) and $1\times TgTau^{+/-}APP^{-/-}$ (Fig. 1e–h). Neither brain atrophy nor hydrocephalus was observed in either group. Progressive accumulation of endogenous mouse tau was also detected by TAU-5 immunostaining in relation to the expressed human tauP301L accumulation. There were no significant differences in brain gliosis, neuronal cell loss, behavioral disturbance, or survival between $2\times TgTau^{+/-}APP^{+/-}$ and $1\times TgTau^{+/-}APP^{-/-}$. However, marked accumulation of phosphorylated tau was detected by AT8 immunostaining in the hippocampus and the cerebral cortices in $2\times TgTau^{+/-}APP^{+/-}$ mice compared with $1\times TgTau^{+/-}APP^{-/-}$ mice at 23 months age (Fig. 1l). This accumulated tau was partially labeled by Gallyas silver stain (see Fig. 2x), suggesting the presence of both pretangles and NFTs in the brains of $2\times TgTau^{+/-}APP^{+/-}$ mice at 23 months of age. Phenotypic variations were also recognized in both $2\times TgTau^{+/-}APP^{+/-}$ and $1\times TgTau^{+/-}APP^{-/-}$ like those in TgTauP301L.

Aβ core plaques labeled by Ab9201 appeared from 8 months of age in both $2\times TgTau^{+/-}APP^{+/-}$ and $1\times TgTau^{-/-}APP^{+/-}$. Numbers and distributions were increased with age in both groups. However, there were no differences in the initiation and distribution of Aβ deposits between $2\times TgTau^{+/-}APP^{+/-}$ (Fig. 1q–t) and $1\times TgTau^{-/-}APP^{+/-}$ (Fig. 1u–x). Furthermore, there were no differences in diffuse Aβ plaques at 16–23 months of age in the two group. From 8 months of age, dystrophic neurites around Aβ cores were present (Fig. 2a). The appearance of phosphorylated tau deposits in dystrophic neurites was enhanced in $2\times TgTau^{+/-}APP^{+/-}$ (Fig. 2c) compared with that in $1\times TgTau^{+/-}APP^{-/-}$ (Fig. 2d). These findings suggested that tauopathy does not induce Aβ amyloidosis, but rather Aβ amyloidosis accelerates phosphorylation and tangle formation of accumulated tau.

Then, phosphorylated tau was examined in detail in the brain of a 23-month-old $2\times TgTau^{+/-}APP^{+/-}$ mouse (Fig. 2e,g,h). Numerous neuropil threads were detected by AT8 staining in the cerebral cortex of the brain (Fig. 2g). There were phosphorylated tau-positive, Gallyas silver stain-negative neurites in the cerebral white matter (Fig. 2h), suggesting the presence of pretangles in the neuronal process. There was no apparent correlation between Aβ amyloid cores and NFTs, as shown in Figure 2i,j. Enhanced GSK-3β staining was also observed (Fig. 2k).

Neurons containing phosphorylated tau-positive pretangles were significantly enhanced and 3.7 times more frequently in the $2\times TgTau^{+/-}APP^{+/-}$ (63%, 5/8) compared with $1\times TgTau^{+/-}APP^{-/-}$ (17%, 5/29) at 23 months of age (Table I, $P = 0.0107$: χ^2 test; Graph Pad Prism 5). Glial tangles were also prominent in the brains of $2\times TgTau^{+/-}APP^{+/-}$: 6/8 (75%) of $2\times TgTau^{+/-}APP^{+/-}$ and 11/29 (38%) of $1\times TgTau^{+/-}APP^{-/-}$ mice ($P = 0.06$). However, there was no significant difference in the incidence of GFTs. Thus, Aβ enhances pretangle formation in neurons and processes.

These pretangles were labeled by antibodies against special phosphorylation sites at serine199 (Fig. 2r), at serine202 (Fig. 2s), at serine202/threonine205 (Fig. 2t), at threonine231/serine235 (Fig. 2u), at serine396/serine404 (Fig. 2v), and at serine413 (Fig. 2w), with conformational changes by MC1 (Fig. 2q) and by Gallyas silver staining (Fig. 2x). These findings correspond to those detected in TgTauP301L and patients with Alzheimer's disease or FTDP-17, suggesting that the appearance, severity, and modifications of accumulated tau are more accelerated by Aβ amyloidosis in $2\times TgTau^{+/-}APP^{+/-}$ than in $1\times TgTau^{+/-}APP^{-/-}$ mice.

To confirm the enhancement and acceleration of tau phosphorylation and NFTs formation, we examined the presence and amounts of sarkosyl-insoluble phosphorylated tau in the $2\times TgTau^{+/-}APP^{+/-}$ and $1\times TgTau^{+/-}APP^{-/-}$ 23-month-old mice by Western blot (Fig. 3). In the first Tris buffer-soluble fractions, human-specific tau antibody HT7 labeled the 66-kD bands. TAU-5 demonstrated 66-kD and 55-kD bands. There were no significant differences in the amounts of human and mouse tau in the Tris-soluble brain fractions of the two groups (Fig. 3a). Almost equal amounts of

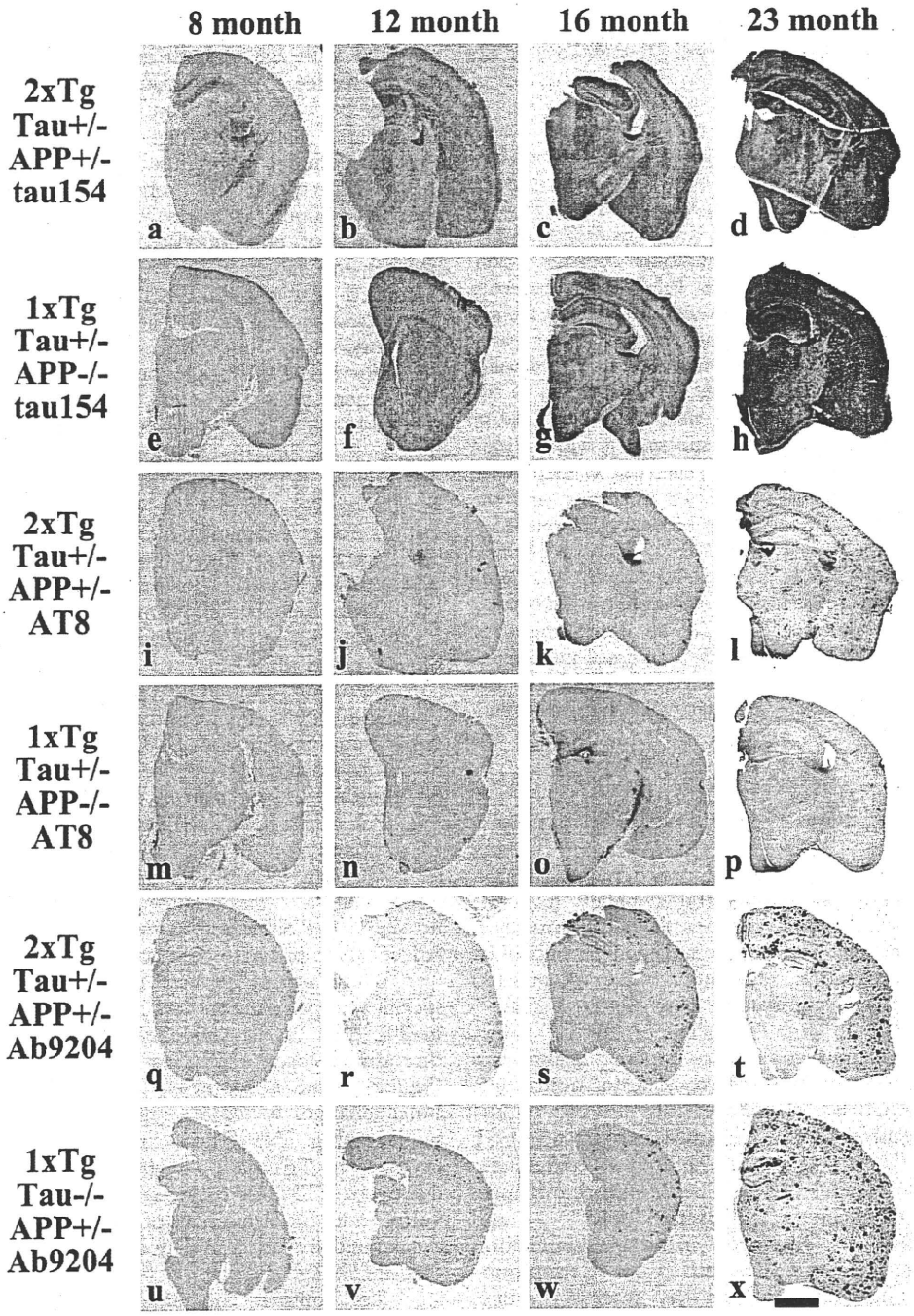

Fig. 1. Time course of accumulation of human tau, phosphorylated tau, and Aβ in 8–23-month-old $2\times TgTau^{+/-}APP^{+/-}$ (**a–d,i–l,q–t**), $1\times Tau^{+/-}APP^{-/-}$ (**e–h,m–p**), and $1\times TgTau^{-/-}APP^{+/-}$ (**u–x**) mice. Mouse sections were stained with tau154 that specifically detects human tau, AT8 for phosphorylated tau at serine202/threonine205, and Ab9204 for Aβ. Scale bar = 800 μm. [Color figure can be viewed in the online issue, which is available at wileyonlinelibrary.com.]

human tau were detected in the sarcosyl-soluble fractions from the brains of both groups (Fig. 3b). However, increased amounts of 66-kD full-length human tauP301L and their 58-kD fragments were increased in the sarkosyl-insoluble brain fraction of $2\times TgTau^{+/-}APP^{+/-}$ compared with those of $1\times TgTau^{+/-}APP^{-/-}$. These

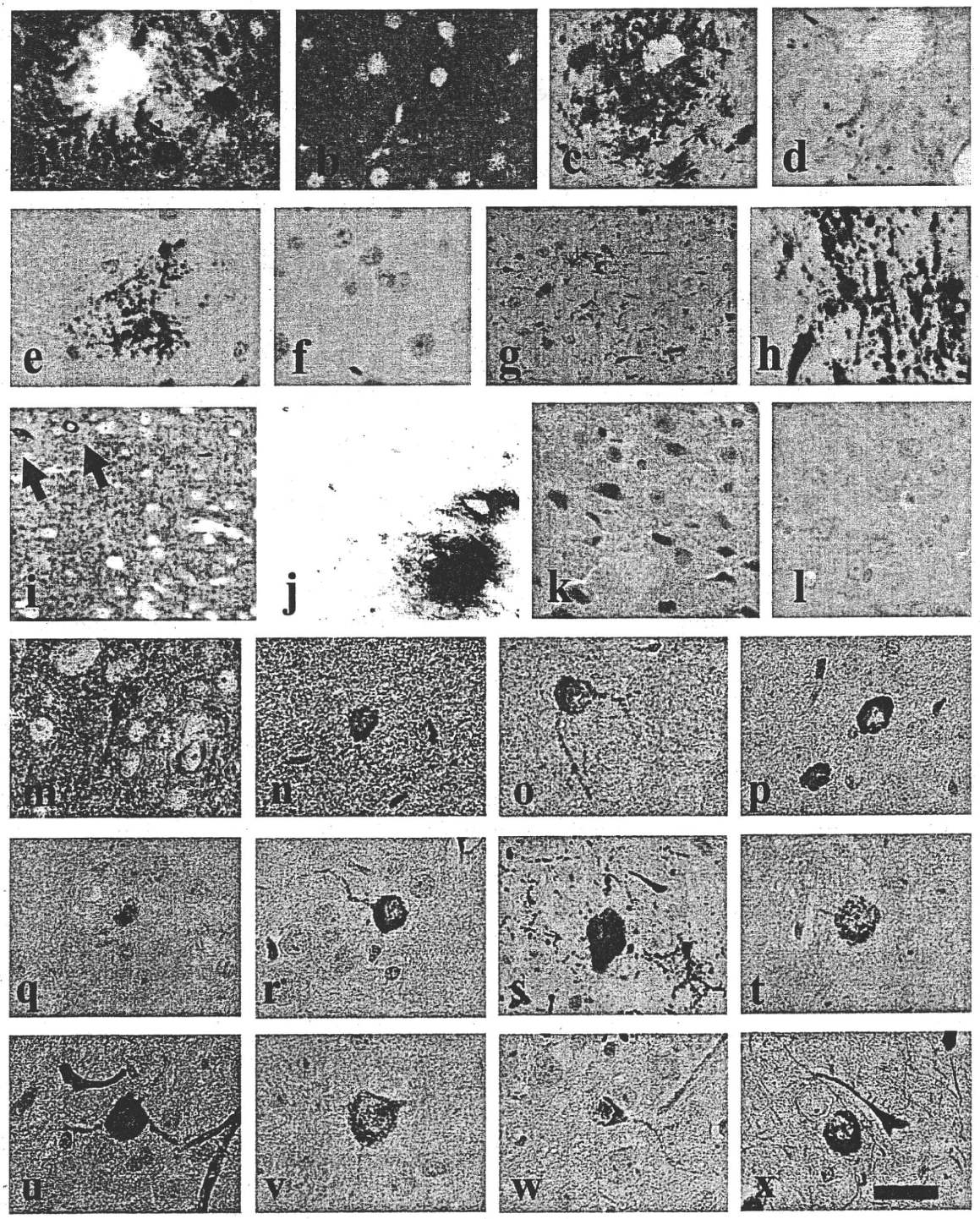

Fig. 2. Immunostaining of $2\times TgTau^{+/-}APP^{+/-}$ (**a,c,e,g–k,m–x**), $1\times TgTau^{+/-}APP^{-/-}$ (**b,f,l**), and $1\times TgTau^{-/-}APP^{+/-}$ (**d**) mice. Sections were stained with tau154 (a,b,i), AT8 (c–h), Ab9204 (j), anti-GSK3β (k,l). Cerebral cortex of $2\times TgTau^{+/-}APP^{+/-}$ was stained anti-tau antibodies; tau-154 (m), HT7 (n), CP27 (o), TAU-5 (p), MC1 (q), anti-PS199 (r), CP13 (s), AT8 (t), anti-PT231/PS235 (u), PHF1 (v), anti-PS413 (w), and Gallyas-Braak stain (x). Scale bar = 12.5 μm. [Color figure can be viewed in the online issue, which is available at wileyonlinelibrary.com.]

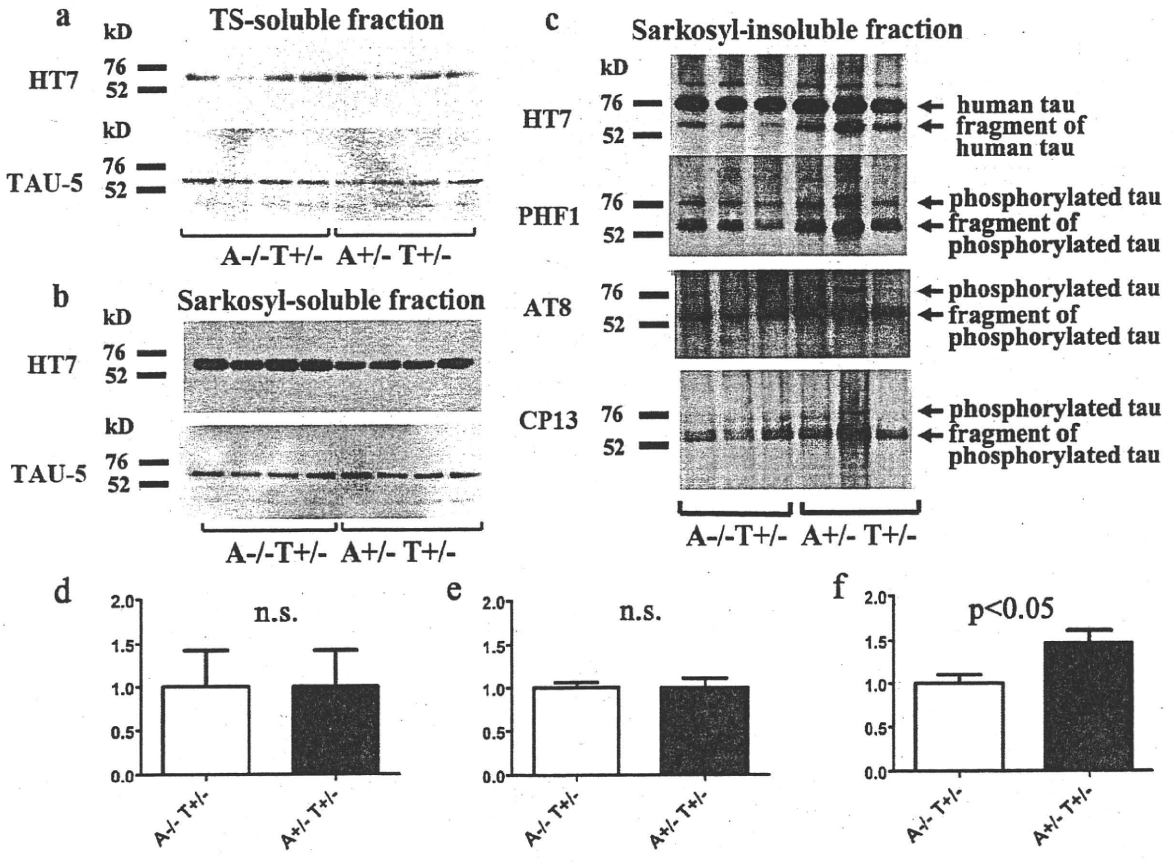

Fig. 3. Western blotting of brain extracts from $2\times TgTau^{+/-}APP^{+/-}$ ($A^{+/-}T^{+/-}$) and $1\times TgTau^{+/-}APP^{-/-}$ ($A^{-/-}T^{+/-}$). **a:** TS-soluble fraction stained with HT7 and TAU-5. **b:** Sarkosyl-soluble fraction stained with HT7 and TAU-5. **c:** Sarcosyl-insoluble fraction stained with HT7, PHF-1, AT8, and CP13. The signal intensity of tau in the sarkosyl-insoluble fraction (**f**) was significantly increased in $2\times TgTau^{+/-}APP^{+/-}$ compared with that in $1\times TgTau^{+/-}APP^{-/-}$; however, that in the TS-soluble fraction (**d**) and sarkosyl-soluble fraction (**e**) did not differ. The mean intensity of the band in $1\times TgTau^{+/-}APP^{-/-}$ is shown as 1.

TABLE I. NFTs and GFTs in $2\times TgTau^{+/-}APP^{+/-}$ and $1\times TgTau^{+/-}APP^{-/-}$

Genotype	$2\times TgTau^{+/-}APP^{+/-}$	$1\times TgTau^{+/-}APP^{-/-}$
Neurofibrillary pretangles	63% (5/8)**	17% (5/29)
Glial fibrillary pretangles	75% (6/8)	38% (11/29)

**$P = 0.0107$.

increased tau isoforms were also labeled by antibody PHF1, AT8, and CP13, suggesting that sarkosyl-insoluble tau is hyperphosphorylated and conformationally changed in the most insoluble brain fractions, which corresponds to those recognized in Alzheimer's disease brains (Fig. 3c). Thus, acceleration of tauopathy in the $2\times TgTau^{+/-}APP^{+/-}$ brain was also detected by biochemical examinations.

DISCUSSION

Both $2\times TgTau^{+/-}APP^{+/-}$ and $1\times TgTau^{+/-}APP^{-/-}$ showed initiation and accumulation of tauP301L starting at 3 months, and those accumulations progressively spread from the hippocampus to the cortices, amygdala, and brainstem. The initial appearance of dystrophic neurites around the core plaques was detected in both mice at the same period of 8 months of age. The number and size of phosphorylated tau were enhanced in dystrophic neurites of $2\times TgTau^{+/-}APP^{+/-}$ mice. Phosphorylated tau-positive pretangles, NFTs, and GFTs and phenotypic variation were also reproduced in both mice. However, the prevalence of mice exhibiting pretangles, NFTs, and phosphorylated tau-positive neuropils was significantly increased in $2\times TgTau^{+/-}APP^{+/-}$ compared with $1\times TgTau^{+/-}APP^{-/-}$ mice at 23 months of age. The distributions of pretangles and NFTs were not correlated with the presence of core plaques. These findings suggest that the presence of Aβ amyloidosis partially enhances the accumulation of phosphorylated tau in neurons and neuronal processes.

Subsequent generation of Aβ plaques and tangles and neurodegeneration have been exhibited by regulatory expression model mice of tauP301L (rTg4510; Spires et al., 2006; Spires-Jones et al., 2008; de Calington et al., 2009) and APPNLI (rTg3696AB; Paulson et al., 2008). In our $2\times TgTau^{+/-}APP^{+/-}$ mice, however, the appearances of pretangles, NFTs, and GFTs were markedly delayed at 23 months of age. Tauopathy was detected at 18 months of age in TgtauP301L, so about a 5-month delay was observed. Florid pathology including brain atrophy, neuronal cell loss, and gliosis detected in TgtauP301L was milder in both $2\times TgTau^{+/-}APP^{+/-}$ and $1\times TgTau^{+/-}APP^{-/-}$ even at 23 months of age. This delay and a milder form of tau pathology were observed in $1\times TgTau^{+/-}APP^{-/-}$, so one possible explanation is that alteration of the genetic background by crossing strains from FBV in TgTauP301L with FVB/B6/SJL occurred in the crossing of double heterozygotes Tg. For this reason, we analyzed many heterozygotes of mice in this study to confirm this phenomenon statistically and to show significant enhancement of tau pathology by Aβ in $2\times TgTau^{+/-}APP^{+/-}$.

Development of Aβ burden was completely identical among $2\times TgTau^{+/-}APP^{+/-}$, $1\times TgTau^{-/-}APP^{+/-}$, and Tg2576. Initial Aβ deposits were detected at 8 months of age, and there was no significant difference in the progressive distribution and density among these three strains. In other double and triple Tg mice, genetically augmented tau levels and hyperphosphorylation in the 3×Tg-AD did not show any effect on the onset and progression of Aβ pathology (Oddo et al., 2007). The somatodendritic tau accumulation is dependent on parenchymal Aβ deposits (Oddo et al., 2009). Aβ-dependent triosephosphate isomerase nitrotyrosination induces glycation and tau fibrillation (Guix et al., 2009). Thus, unidirectional facilitation of tauopathy by Aβ amyloidosis and Aβ oligomer was considered (Oddo et al., 2006b). The initial alteration of Tg2576 brain was Aβ dimers in lipid rafts at 6 months of age, and subsequent accumulation of phosphorylated tau was identified (Kawarabayashi et al., 2004). Because enhancement of pretangles, NFTs and GTFs appeared in the late stage of Aβ burden consisting of many core plaques and diffuse plaques, the acceleration effect of tauopathy by Aβ amyloid is not considered very strong, but the incubation period seems to be long despite previous findings regarding the mutant presenilin-1 effect on APP double Tg mice (Holcomb et al., 1998).

As clearly shown in TgtauP301L, many tau transgenic mice exhibited loss of neurons and synapses. Accumulation of tau in axonal defects was an early event in the brains of AD and APP Tg mice (Stokin et al., 2005). Suppression of tau expression in mice expressing a repressible tauP301L developing progressive NFTs, neuronal cell loss, and behavioral impairments recovered memory function and neuron numbers (Santacruz et al., 2005). Transgenic TAU zebrafish clearly showed that GSK3β-mediated NFT formation actually induces neuronal cell death (Paquet et al., 2009). Neurotoxicity induced by fibrillar Aβ on hippocampal cultured neurons is mediated by tau (Rapoport et al., 2002). There was no neuronal cell loss or synaptic losses at 23 months of age in $2\times TgTau^{+/-}APP^{+/-}$. These findings indicated that an NFT burden more severe than that shown in $2\times TgTau^{+/-}APP^{+/-}$ is necessary to induce neuronal cell loss and that Aβ amyloid fibrils and oligomer were not sufficient to induce this neurodegenerative processes.

Other double transgenic mice obtained by crossing Tg2576 and tau transgenic mice expressing tauG272V, P301L, and R406W showed an increase in tau phosphorylation at serine262 and -422 (Pérez et al., 2005). Lithium, a well-known drug that inhibits GSK-3 activities, reduced tau phosphorylation but did not alter the Aβ load (Caccamo et al., 2007). Injection of Aβ42 fibrils into the brains of tauP301L transgenic mice caused a fivefold increase in the number of NFTs in the amygdala where neurons projected to the injected site, 18 days after Aβ42 injection (Götz et al., 2001). Amyloid induces tauopathy through activation of GSK-3β in APP-V717I × TauP301L mice (Terwel et al., 2008). Tau reduction can block Aβ and excitotoxin-induced neuronal dysfunction (Robertson et al., 2007). All these findings indicate that Aβ might induce NFTs through phosphorylation of tau and formation of conformationally changed tau and GSK3β activation. In accordance with these findings, $2\times TgTau^{+/-}APP^{+/-}$ showed enhanced phosphorylation at serine199, at serine202, at serine202/threonine205, at threonine231/serine235, at serine 396/serine404, and at serine413 and the presence of conformational alteration and argylophilic properties as well as increased expression of GSK-3β. Biochemical analysis further confirmed the histological findings and indicated that this hyperphosphorylated and conformationally changed tau acutully gains insolubility, leading to accumulation of aggregated tau in the sarkosyl-insoluble fraction in the brain.

In summary, enhancement of tauopathy by Aβ may partially initiate pretangle formation in the neuronal processes and cytoplasm. Based on the presence of many pretangles in the cortex, NFTs and GFTs emerged. These findings correspond to conventional neuropathological findings and other reports on AD model mice (LaFerla and Oddo, 2005, Spires-Jones et al., 2009). Our data and these reports support the hypothesis that disturbance of axonal transport of phosphorylated tau in the axons is an early event induced by Aβ amyloid deposition. Further drug development targeting this step would be desirable.

ACKNOWLEDGMENTS

We thank K. Sato, M. Ono, K. Iinuma, Y. Sato, R. Tushima, and I. Shirahama for technical assistance; Dr. TC Saido for generously donating Ab9204; Dr. Peter Davies for CP27, CP13, MC1, and PHF-1 antibodies; and Dr. Koich Ishiguro for tau-154, PS199, anti-PT231/PS235, anti-PS413, anti-GSK3β antibodies.

REFERENCES

Caccamo A, Oddo S, Tran LX, LaFerla FM. 2007. Lithium reduces tau phosphorylation but not Aβ or working memory deficits in a transgenic model with both plaques and tangles. Am J Pathol 170:1669–1675.

de Calignon A, Spires-Jones TL, Pitstick R, Carlson GA, Hyman BT. 2009. Tangle-bearing neurons survive despite disruption of membrane

integrity in a mouse model of tauopathy. J Neuropathol Exp Neurol 68:757–761.

Ghiso JA, Holton J, Miravalle L, Calero M, Lashley T, Vidal R, Houlden H, Wood N, Neubert TA, Rostagno A, Plant G, Revesz T, Frangione B. 2001. Systemic amyloid deposits in familial British dementia. J Biol Chem 276:43909–43914.

Götz J, Chen F, van Dorpe J, Nitsch RM. 2001. Formation of neurofibrillary tangles in P301L tau transgenic mice induced by Aβ42 fibrils. Science 293:1491–1495.

Guix FX, Ill-Raga G, Bravo R, Nakaya T, de Fabritiis G, Coma M, Miscione GP, Villà-Freixa J, Suzuki T, Fernàndez-Busquets X, Valverde MA, de Strooper B, Muñoz FJ. 2009. Amyloid-dependent triosephosphate isomerase nitrotyrosination induces glycation and tau fibrillation. Brain 132:1335–1345.

Hardy J. 2009. The amyloid hypothesis for Alzheimer's disease: a critical reappraisal. J Neurochem 110:1129–1134.

Holcomb L, Gordon MN, McGowan E, Yu X, Benkovic S, Jantzen P, Wright K, Saad I, Mueller R, Morgan D, Sanders S, Zehr C, O'Campo K, Hardy J, Prada CM, Eckman C, Younkin S, Hsiao K, Duff K. 1998. Accelerated Alzheimer-type phenotype in transgenic mice carrying both mutant amyloid precursor protein and presenilin 1 transgenes. Nat Med 4:97–100.

Holmes C, Boche D, Wilkinson D, Yadegarfar G, Hopkins V, Bayer A, Jones RW, Bullock R, Love S, Neal JW, Zotova E, Nicoll JA. 2008. Long-term effects of Aβ42 immunization in Alzheimer's disease: follow-up of a randomised, placebo-controlled phase I trial. Lancet 372:216–223.

Hutton M, Lendon CL, Rizzu P, Baker M, Froelich S, Houlden H, Pickering-Brown S, Chakraverty S, Isaacs A, Grover A, Hackett J, Adamson J, Lincoln S, Dickson D, Davies P, Petersen RC, Stevens M, de Graaff E, Wauters E, van Baren J, Hillebrand M, Joosse M, Kwon JM, Nowotny P, Che LK, Norton J, Morris JC, Reed LA, Trojanowski J, Basun H, Lannfelt L, Neystat M, Fahn S, Dark F, Tannenberg T, Dodd PR, Hayward N, Kwok JB, Schofield PR, Andreadis A, Snowden J, Craufurd D, Neary D, Owen F, Oostra BA, Hardy J, Goate A, van Swieten J, Mann D, Lynch T, Heutink P. 1998. Association of missense and 5′-splice-site mutations in tau with the inherited dementia FTDP-17. Nature 393:702–705.

Kawarabayashi T, Shoji M, Younkin LH, Wen-Lang L, Dickson DW, Murakami T, Matsubara E, Abe K, Ashe KH, Younkin SG. 2004. Dimeric amyloid β protein rapidly accumulates in lipid rafts followed by apolipoprotein E and phosphorylated tau accumulation in the Tg2576 mouse model of Alzheimer's disease. J Neurosci 24:3801–3809.

LaFerla FM, Oddo S. 2005. Alzheimer's disease: Aβ, tau and synaptic dysfunction. Trends Mol Med 11:170–176.

Lewis J, Dickson DW, Lin WL, Chisholm L, Corral A, Jones G, Yen SH, Sahara N, Skipper L, Yager D, Eckman C, Hardy J, Hutton M, McGowan E. 2001. Enhanced neurofibrillary degeneration in transgenic mice expressing mutant tau and APP. Science 293:1487–1491.

Love S, Bridges LR, Case CP. 1995. Neurofibrillary tangles in Niemann-Pick disease type C. Brain 118:119–129.

Murakami T, Paitel E, Kawarabayashi T, Ikeda M, Chishti MA, Janus C, Matsubara E, Sasaki A, Kawarai T, Phinney AL, Harigaya Y, Horne P, Egashira N, Mishima K, Hanna A, Yang J, Iwasaki ,K, Takahashi M, Fujiwara M, Ishiguro K, Bergeron C, Carlson GA, Abe K, Westaway D, St. George-Hyslop P, Shoji M. 2006. Cortical neuronal and glial pathology in TgTauP301L transgenic mice: neuronal degeneration, memory disturbance, and phenotypic variation, Am J Pathol 169:1365–1375.

Oddo S, Billings L, Kesslak JP, Cribbs DH, LaFerla FM. 2004. Aβ immunotherapy leads to clearance of early, but not late, hyperphosphorylated tau aggregates via the proteasome. Neuron 43:321–332.

Oddo S, Vasilevko V, Caccamo A, Kitazawa M, Cribbs DH, LaFerla FM. 2006a. Reduction of soluble Aβ and tau, but not soluble Aβ alone, ameliorates cognitive decline in transgenic mice with plaques and tangles. J Biol Chem 281:39413–39423.

Oddo S, Caccamo A, Tran L, Lambert MP, Glabe CG, Klein WL, LaFerla FM. 2006b. Temporal profile of amyloid-β (Aβ) oligomerization in an in vivo model of Alzheimer disease. A link between Aβ and tau pathology. J Biol Chem 281:1599–1604.

Oddo S, Caccamo A, Cheng D, Jouleh B, Torp R, LaFerla FM. 2007. Genetically augmenting tau levels does not modulate the onset or progression of Aβ pathology in transgenic mice. J Neurochem 102:1053–1063.

Oddo S, Caccamo A, Tseng B, Cheng D, Vasilevko V, Cribbs DH, LaFerla FM. 2008. Blocking Aβ42 accumulation delays the onset and progression of tau pathology via the C terminus of heat shock protein70-interacting protein: a mechanistic link between Aβ and tau pathology. J Neurosci 28:12163–12175.

Oddo S, Caccamo A, Cheng D, LaFerla FM. 2009. Genetically altering Aβ distribution from the brain to the vasculature ameliorates tau pathology. Brain Pathol 19:421–430.

Paquet D, Bhat R, Sydow A, Mandelkow EM, Berg S, Hellberg S, Fälting J, Distel M, Köster RW, Schmid B, Haass C. 2009. A zebrafish model of tauopathy allows in vivo imaging of neuronal cell death and drug evaluation. J Clin Invest 119:1382–1395.

Paulson JB, Ramsden M, Forster C, Sherman MA, McGowan E, Ashe KH. 2008. Amyloid plaque and neurofibrillary tangle pathology in a regulatable mouse model of Alzheimer's disease. Am J Pathol 173:762–772.

Pérez M, Ribe E, Rubio A, Lim F, Morán MA, Ramos PG, Ferrer I, Isla MT, Avila J. 2005. Characterization of a double (amyloid precursor protein-tau) transgenic: tau phosphorylation and aggregation. Neuroscience 130:339–347.

Rapoport M, Dawson HN, Binder LI, Vitek MP, Ferreira A. 2002. Tau is essential to β-amyloid-induced neurotoxicity. Proc Natl Acad Sci U S A 99:6364–6369.

Roberson ED, Scearce-Levie K, Palop JJ, Yan F, Cheng IH, Wu T, Gerstein H, Yu GQ, Mucke L. 2007. Reducing endogenous tau ameliorates amyloid β-induced deficits in an Alzheimer's disease mouse model. Science 316:750–754.

Santacruz K, Lewis J, Spires T, Paulson J, Kotilinek L, Ingelsson M, Guimaraes A, DeTure M, Ramsden M, McGowan E, Forster C, Yue M, Orne J, Janus C, Mariash A, Kuskowski M, Hyman B, Hutton M, Ashe KH. 2005. Tau suppression in a neurodegenerative mouse model improves memory function. Science 309:476–481.

Spires TL, Orne JD, SantaCruz K, Pitstick R, Carlson GA, Ashe KH, Hyman BT. 2006. Region-specific dissociation of neuronal loss and neurofibrillary pathology in a mouse model of tauopathy. Am J Pathol 168:1598–1607.

Spires-Jones TL, de Calignon A, Matsui T, Zehr C, Pitstick R, Wu HY, Osetek JD, Jones PB, Bacskai BJ, Feany MB, Carlson GA, Ashe KH, Lewis J, Hyman BT. 2008. In vivo imaging reveals dissociation between caspase activation and acute neuronal death in tangle-bearing neurons. J Neurosci 28:862–867.

Spires-Jones TL, Stoothoff WH, de Calignon A, Jones PB, Hyman BT. 2009. Tau pathophysiology in neurodegeneration: a tangled issue. Trends Neurosci 32:150–159.

Stokin GB, Lillo C, Falzone TL, Brusch RG, Rockenstein E, Mount SL, Raman R, Davies P, Masliah E, Williams DS, Goldstein LS. 2005. Axonopathy and transport deficits early in the pathogenesis of Alzheimer's disease. Science 307:1282–1288.

Terwel D, Muyllaert D, Dewachter I, Borghgraef P, Croes S, Devijver H, Van Leuven F. 2008. Amyloid activates GSK-3β to aggravate neuronal tauopathy in bigenic mice. Am J Pathol 172:786–798.

Tomidokoro Y, Ishiguro K, Harigaya Y, Matsubara E, Ikeda M, Park JM, Yasutake K, Kawarabayashi T, Okamoto K, Shoji M. 2001. Aβ amyloidosis induces the initial stage of tau accumulation in APP(Sw) mice. Neurosci Lett 299:169–172.

THE JOURNAL OF BIOLOGICAL CHEMISTRY VOL. 286, NO. 8, pp. 6393–6401, February 25, 2011

Lipoprotein Lipase Is a Novel Amyloid β (Aβ)-binding Protein That Promotes Glycosaminoglycan-dependent Cellular Uptake of Aβ in Astrocytes*[S]

Received for publication, August 4, 2010, and in revised form, November 23, 2010 Published, JBC Papers in Press, December 21, 2010, DOI 10.1074/jbc.M110.172106

Kazuchika Nishitsuji[‡], Takashi Hosono[‡], Kenji Uchimura[‡§], and Makoto Michikawa[‡1]

From the [§]Section of Pathophysiology and Neurobiology, [‡]Department of Alzheimer's Disease Research, National Center for Geriatrics and Gerontology, Obu, Aichi 474-8511, Japan

Lipoprotein lipase (LPL) is a member of a lipase family known to hydrolyze triglyceride molecules in plasma lipoprotein particles. LPL also plays a role in the binding of lipoprotein particles to cell-surface molecules, including sulfated glycosaminoglycans (GAGs). LPL is predominantly expressed in adipose and muscle but is also highly expressed in the brain where its specific roles are unknown. It has been shown that LPL is colocalized with senile plaques in Alzheimer disease (AD) brains, and its mutations are associated with the severity of AD pathophysiological features. In this study, we identified a novel function of LPL; that is, LPL binds to amyloid β protein (Aβ) and promotes cell-surface association and uptake of Aβ in mouse primary astrocytes. The internalized Aβ was degraded within 12 h, mainly in a lysosomal pathway. We also found that sulfated GAGs were involved in the LPL-mediated cellular uptake of Aβ. Apolipoprotein E was dispensable in the LPL-mediated uptake of Aβ. Our findings indicate that LPL is a novel Aβ-binding protein promoting cellular uptake and subsequent degradation of Aβ.

Lipoprotein lipase (LPL)[2] catalyzes the hydrolysis of triacylglycerol and mediates the cellular uptake of lipoproteins by functioning as a "bridging molecule" between lipoproteins and sulfated glycosaminoglycans (GAGs) or lipoprotein receptors in blood vessels (1, 2). Sulfated GAGs are side chains of proteoglycans normally found in the extracellular matrix and on the cell surface in the peripheral tissues and brain. Sulfation modifications vary within the GAG chains and are crucial for interaction between GAGs and various protein ligands (3), including LPL (4, 5).

It has been shown that LPL is distributed in numerous organs and is highly expressed in the brain (6, 7). Although the catabolic activity of LPL on triacylglycerol is observed in the brain (8), the finding that apolipoprotein CII (apoCII), an essential cofactor for LPL, is not expressed in the brain (9, 10), suggests that LPL has a novel nonenzymatic function in the brain. However, little is known about LPL function in the brain. Interestingly, it has been shown that LPL is accumulated in senile plaques of Alzheimer disease (AD) brains (11). Moreover, SNPs in the coding region of the LPL gene are associated with disease incidence in clinically diagnosed AD subjects, LPL mRNA expression level, brain cholesterol level, and the severity of AD pathologies, including neurofibrillary tangles and senile plaque density (12). These results suggest that LPL may have a physiological role in the brain, whose alternation is associated with the pathogenesis of AD.

The occurrence of senile plaques in the brain is one of the pathological hallmarks of AD. They contain extracellular deposits of amyloid β protein (Aβ), and the abnormal Aβ deposition or the formation of soluble Aβ oligomers is crucial for AD pathogenesis. Aβ is a physiological peptide whose main species are 40 and 42 amino acids in length, and Aβ42 is the predominant specie in senile plaques (13). The Aβ levels are determined by the balance between its production and degradation/clearance, and an attenuated Aβ catabolism is suggested to cause Aβ accumulation in aging brains (14). Previous studies have shown that astrocytes and microglia directly take up and degrade Aβ42 (15, 16) and that Aβ degradation occurs in late endosomal-lysosomal compartments (17, 18). These lines of evidence, together with the finding that LPL mediates the cellular uptake of lipoproteins (1, 2), led us to carry out experiments to determine whether LPL interacts with Aβ to promote Aβ cellular uptake and degradation in astrocytes. Here, we provide evidence that LPL forms a complex with Aβ and facilitates Aβ cell surface binding and uptake in mouse primary astrocytes through a mechanism that is dependent on heparan sulfate and chondroitin sulfate GAG chains, leading to the lysosomal degradation of Aβ.

MATERIALS AND METHODS

Materials—Bovine LPL, heparinases, and a polyclonal anti-actin antibody were purchased from Sigma. Synthetic Aβ1–42 was purchased from the Peptide Institute (Osaka,

* This work was supported by a grant-in-aid for scientific research on priority areas (Research on Pathomechanisms of Brain Disorders) from the Ministry of Education, Culture, Sports, Science, and Technology of Japan, a grant from the Program for Promotion of Fundamental Studies in Health Sciences of the National Institute of Biomedical Innovation, a grant from the Ministry of Health, Labor, and Welfare of Japan (Research on Dementia, Health, and Labor Sciences Research Grant H20-007), and a grant from the Japan Health Sciences Foundation (Research on Publicly Essential Drugs and Medical Devices).

[S] The on-line version of this article (available at http://www.jbc.org) contains supplemental "Methods" and Fig. 1.

[1] To whom correspondence should be addressed: Department of Alzheimer's Disease Research, National Center for Geriatrics and Gerontology, Gengo 35, Morioka, Obu, Aichi 474-8511, Japan. Tel.: 81-562-46-2311; Fax: 81-562-46-8569; E-mail: michi@ncgg.go.jp.

[2] The abbreviations used are: LPL, lipoprotein lipase; Aβ, amyloid β; ApoE, apolipoprotein E; CS, chondroitin sulfate(s); HS, heparan sulfate; GAG, glycosaminoglycan; ANOVA, one-way analysis of variance.

Japan). Heparin, chondroitin, chondroitin sulfates, and chondroitinase ABC were from Seikagaku (Tokyo, Japan). Monoclonal anti-Aβ antibodies (6E10, 4G8) were purchased from Signet Laboratories (Dedham, MA), and a goat polyclonal anti-ApoE antibody and mouse control IgG were from Millipore (Bedford, MA). An anti-LPL antibody and Cy3- and FITC- conjugated secondary antibodies were purchased from Abcam, Inc. (Cambridge, MA). A monoclonal anti-Aβ antibody (2C8) was purchased from Medical and Biological Laboratories (Nagoya, Japan).

Animals—C57BL/6 mice were purchased from SLC, Inc. (Hamamatsu, Japan). ApoE-KO mice were obtained from Jackson ImmunoResearch Laboratories (Bar Harbor, ME). The National Center of Geriatrics and Gerontology Institutional Animal Care and Use Committee approved the animal studies.

Preparation of LPL—Because the sequence of LPL is highly conserved among mammalian species and the ability of LPL to interact with proteoglycans is also well conserved, we used LPL purified from bovine milk. An LPL suspension (suspended in 3.8 M ammonium sulfate, 0.02 M Tris-HCl, pH 8.0) was centrifuged (10,000 × *g* for 20 min at 4 °C), and the resulting pellet was dissolved in PBS. The prepared LPL was stored at 4 °C and used within 3 days.

Cell Culture—Highly astrocyte-rich cultures were prepared according to a method described previously (19). In brief, brains of postnatal day 2 C57BL/6 mice or ApoE knock-out mice were removed under anesthesia. The cerebral cortices from the mouse brains were dissected, freed from meninges, and diced into small pieces; the cortical fragments were incubated in 0.25% trypsin and 20 mg/ml DNase I in PBS at 37 °C for 20 min. The fragments were then dissociated into single cells by pipetting. The dissociated cells were seeded in 75-cm^2 dishes at a density of 5×10^7 cells per flask in DMEM-containing 10% FBS. After 10 days of incubation *in vitro*, flasks were shaken at 37 °C overnight, and the remaining astrocytes in the monolayer were trypsinized (0.1%) and reseeded. The astrocyte-rich cultures were maintained in DMEM-containing 10% FBS until use.

Assay of Aβ Binding and Uptake in Astrocytes by Western Blotting—Assays were carried out on confluent monolayers of astrocytes grown in 12-well plates. Aβ was dissolved in dimethyl sulfoxide to a final concentration of 1 mM and stored at −40 °C. Aβ (500 nM) and LPL (1–10 μg/ml) were mixed in DMEM. Immediately, the mixture was added to the culture medium of astrocytes. Cells were incubated at 37 °C for 5 h to assess the cellular uptake of Aβ or at 4 °C for 3 h to evaluate the binding of Aβ to the cell surface of astrocytes. In these assays, cells were incubated in serum-free DMEM. After incubation, cells were washed with PBS three times, harvested using a cell scraper and lysed by sonication in radioimmune precipitation assay buffer (1% Nonidet P-40, 0.5% sodium deoxycholate, 0.1% SDS, 150 mM NaCl, 50 mM Tris-HCl (pH 8.0), 1 mM EDTA). Cell lysates were subjected to SDS-PAGE with 4–20% gradient gels (WAKO Pure Chemicals, Osaka, Japan) and transferred to polyvinylidene difluoride membranes (Millipore). Aβ was probed with 6E10 antibody followed by horseradish peroxidase-labeled anti-mouse antibody (Cell Signaling Technology, Inc., Beverly, MA) and chemiluminescent substrate ECL Plus (GE Healthcare). The protein contents of cell lysates were normalized to the expression level of actin protein. To examine the involvement of GAGs, heparin, chemically modified heparins, chondroitin, or chondroitin sulfates (3 μg/ml) were incubated with a mixture solution of Aβ and LPL. Astrocytes were pretreated with a mixture of heparinase II and heparinase III or chondroitinase ABC (0.03 units/ml) for 24 h at 37 °C to evaluate endogenously expressed glycosaminoglycans. Signals were visualized and quantified using a LAS-3000 luminescent image analyzer (Fujifilm, Tokyo, Japan) and ImageJ software (National Institutes of Health, Bethesda, MD). For analyzing protein band densities, a region of interest was drawn around a band, and protein band densities were calculated.

siRNA Interference of LPL—siRNA specific for mouse LPL (sense strand, 5′-CAGCUGAGGACACUUGUCAUCUCAUdTdT-3′; antisense strand, 5′-AUGAGAUGACAAGUGUCCUCAGCUGdTdT-3′) and control siRNA (sense strand, 5′-CAGAGGGCACAUUUGACCUUUCCAUdTdT-3′; antisense strand, 5′-AUGGAAAGGUCAAAUGUGCCCUCUG-3′) was purchased from Invitrogen. Astrocytes grown in 12-well plates for 24 h were transfected with either LPL siRNA or control siRNA with Lipofectamine RNAiMAX (Invitrogen). Forty-eight hours after transfection, cells were treated with Aβ (1 μM) and then incubated at 4 °C for 3 h, and cell-surface associated Aβ was analyzed as described above. An anti-LPL antibody (Gene Tex, Inc.) was used for the detection of LPL.

Assay of Aβ Degradation in Astrocytes—Astrocytes were incubated with Aβ (250 nM) and LPL (2 μg/ml) at 37 °C for 5 h. Subsequently, cells were washed with DMEM and incubated in DMEM for additional hours. Then, Aβ in cell lysates was analyzed by Western blotting as described above.

Immunoprecipitation—Aβ (500 nM) and LPL at various concentrations were incubated in DMEM at 37 °C for 3 h. LPL-Aβ complexes were immunoprecipitated with an anti-LPL antibody and magnetic protein G beads (Dynal, Hamburg, Germany). For detection of LPL-Aβ complexes in the mice brains, brain homogenates from 12-week-old C57BL/6 mice were used. In brief, anesthetized mice were perfused with PBS containing 35 μg/ml heparin for 15 min. The cerebrum was dissected out and homogenized by sonication in 4 volumes of PBS containing a protease inhibitor mixture (P8340; Sigma) and centrifuged at 1,000 × *g* for 10 min at 4 °C. The supernatants were harvested and LPL-Aβ complexes were immunoprecipitated with an anti-LPL antibody and magnetic protein G beads. The obtained precipitates were washed three times with PBS and incubated at 70 °C for 10 min in SDS sample buffer. Dissociated Aβ recovered in the supernatant was assessed by Western blotting as described above. For detection of endogenous Aβ, the supernatants were subjected to SDS-PAGE with 4–20% gradient gels and transferred to polyvinylidene difluoride membranes. The membranes were exposed to microwave irradiation for 20 s, and Aβ was probed with 4G8 antibody followed by horseradish peroxidase-labeled anti-mouse antibody and the chemiluminescent substrate ECL Plus.

Immunocytochemistry—Astrocytes grown on poly-L-lysine-coated coverslips were incubated with a mixture of Aβ (250 nM) and LPL (2 μg/ml) at 37 °C for 5 h. After treatment, the cells were fixed with 4% paraformaldehyde in PBS at room temperature for 10 min, blocked, and permeabilized with 10% normal goat serum and 0.05% saponin in PBS at room temperature for 20 min. In some experiments, cells were washed twice with DMEM followed by incubation at 37 °C for 3 h in DMEM and fixed. The cells were then incubated with primary antibodies followed by Cy3- and FITC-conjugated secondary antibodies. The stained specimens were mounted with Fluor-Save reagents (Calbiochem) and examined under an LSM 510 confocal laser microscope (Carl Zeiss MicroImaging GmbH, Jena, Germany).

Statistical Analysis—The collected data were analyzed by one-way analysis of variance (ANOVA) including appropriate variables followed by the Dunnett's test or unpaired Student's *t* test. Results were considered significant when $p < 0.05$.

RESULTS

LPL Binds to Aβ in Vitro—LPL was incubated with freshly prepared Aβ42 *in vitro*, and the complexes formed were immunoprecipitated with an anti-LPL antibody coupled with magnetic beads, followed by probing Western blots of protein complexes using an anti-Aβ antibody (Fig. 1*A*). Aβ42 was immunoprecipitated with an anti-LPL antibody, but not with control IgG. The levels of Aβ42 recovered in the immunoprecipitates from samples in the presence of 2–5 μg/ml LPL were significantly higher than those from samples in the presence of 0, 0.5, or 1 μg/ml of LPL (Fig. 1, *B* and *C*), suggesting that LPL directly interacts with Aβ42, and these two molecules form a complex in an LPL dose-dependent manner. Furthermore, endogenous mouse Aβ was immunoprecipitated with the anti-LPL antibody from brain homogenates prepared from C57BL/6 mice (Fig. 1*D*), indicating that endogenous mouse LPL directly interacts with endogenous mouse Aβ. We also determined the assembly state of Aβ that forms complex with LPL. Solutions containing Aβ oligomers were subjected to immunoprecipitation/immunoblot analysis, and Aβ42 monomers were immunoprecipitated by an anti-LPL antibody (supplemental Fig. 1).

LPL Promotes Cell Surface Binding and Cellular Uptake of Aβ in Astrocytes—We then determined whether LPL affects the cellular binding of Aβ to astrocytes. Soluble Aβ42 and various concentrations of LPL were added to primarily cultured astrocytes prepared from WT mice and then incubated at 4 °C. LPL (2–5 μg/ml) of significantly augmented Aβ42 binding to astrocytes by 5.8- to 9-fold of that in the case without LPL (Fig. 2, *A* and *B*). To examine the effect of LPL on the cellular uptake of Aβ, we incubated primary astrocytes with soluble Aβ42 at 37 °C for 5 h. Apparently, the level of Aβ uptake by astrocytes increased in the presence of LPL at concentrations of 2 to 5 μg/ml (Fig. 2*C*, lysate). Consistent with the increase in the level of cellular uptake of Aβ, the level of Aβ remaining in culture medium was decreased (Fig. 2*C*, medium). The Aβ levels in the cell lysate quantified are shown in Fig. 2*D*, indicating that Aβ levels were significantly increased by 5–8-fold that in astrocytes incubated without LPL. Next,

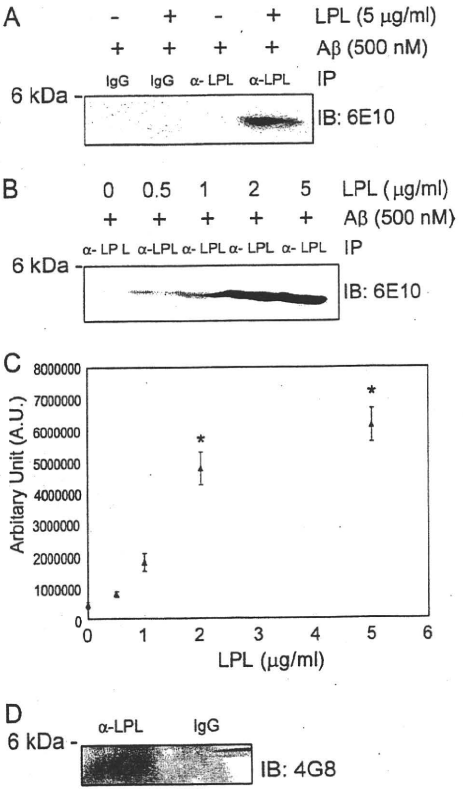

FIGURE 1. **LPL binds to Aβ *in vitro*.** *A*, LPL (5 μg/ml) and Aβ (500 nM) were incubated in DMEM at 37 °C for 3 h. Protein complexes formed were immunoprecipitated with an anti-LPL antibody (α-LPL), and the immunoprecipitates (*IP*) were analyzed by Western blotting using 6E10, an anti-Aβ antibody. These data are representative of three independent experiments. *B*, LPL at various concentrations of 0, 0.5, 1, 2, and 5 μg/ml and Aβ at 500 nM were incubated in DMEM at 37 °C for 3 h. Protein complexes formed were immunoprecipitated with an α-LPL, and the immunoprecipitates were subjected to Western blotting using 6E10. *C*, quantification of Aβ immunoprecipitated with α-LPL. The data presented are the means ± S.D. of three independent experiments. *, $p < 0.001$ *versus* samples without LPL treatment. *D*, the mouse cerebrum was homogenized by sonication in 4 volumes of PBS containing a protease inhibitor mixture and centrifuged at 1000 × *g* for 10 min at 4 °C. The supernatants were harvested. LPL-Aβ complexes in the supernatant were immunoprecipitated with an α-LPL, and the Aβ in the immunoprecipitates was detected by Western blotting using 4G8, an anti-Aβ antibody. *IB*, immunoblot.

we determined the time-dependent effect of LPL-mediated Aβ uptake into astrocytes. Astrocyte cultures were incubated with Aβ (500 nM) and LPL (2 μg/ml) at 37 °C for various hours, and the Aβ level in the cell lysate was determined. The level of Aβ in the cell lysate increased in a time-dependent manner (Fig. 2*E*). The Aβ levels in the astrocytes incubated for 3 and 5 h were significantly higher by 9–14-fold of that in astrocytes incubated without LPL (Fig. 2*F*). These concentrations of LPL are comparable with the concentrations with which LPL could act as "bridging molecules" (2, 20). There were no significant differences among the values for cultures without LPL (one-way ANOVA, $p = 0.1386$). No change in cellular morphology or cell number in astrocyte cultures was observed during the incubation (data not shown). To examine the involvement of LPL expressed by astrocytes, we carried out experiments using the gene silencing technique for LPL. The transient knockdown of LPL expression was achieved by the transfection of siRNA specific for LPL. After transfection,

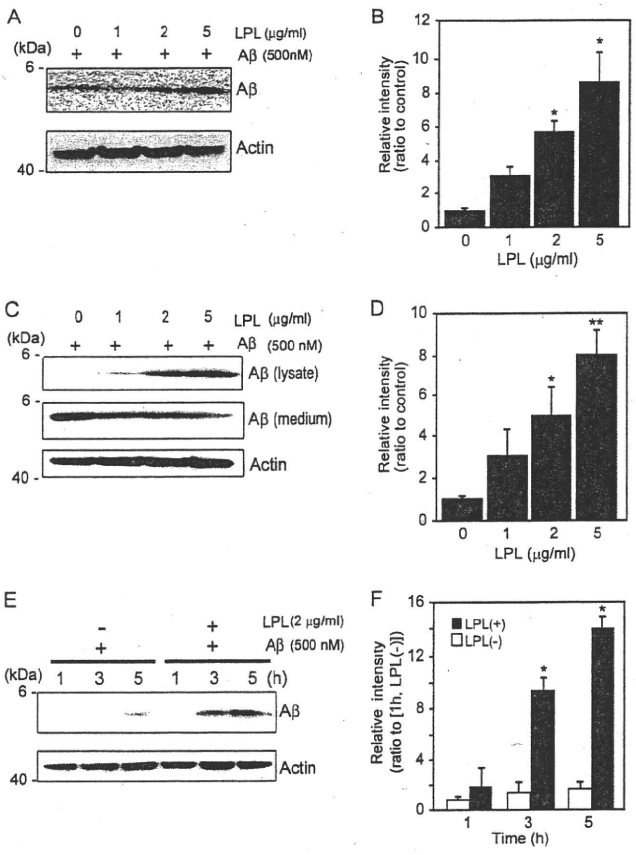

FIGURE 2. **LPL augments cell-surface association and cellular uptake of Aβ in astrocytes.** *A*, mouse primary astrocytes were incubated with LPL (0–5 μg/ml) and Aβ (500 nM) at 4 °C for 3 h. The astrocytes were washed in cold PBS three times, and the cells were harvested using a scraper. The level of Aβ on the cell surface was determined by Western blotting in a detergent extract of whole cells. *B*, quantification of cell-surface-associated Aβ. The data are the means ± S.D. of three independent experiments. *, $p < 0.001$ *versus* LPL at 0 μg/ml. *C* and *D*, astrocytes were incubated with Aβ (500 nM) and LPL (0, 1, 2, and 5 μg/ml) at 37 °C for 3 h. The cultured cells were then washed thoroughly in PBS for three times, and the cells were collected. The level of Aβ in the whole cell lysate (*lysate*), and the conditioned medium of cultured cells (*medium*) were determined by Western blotting using 6E10 antibody. The level of actin demonstrated by Western blotting using an anti-β-actin antibody was used as the loading control. These data are representative of at least three independent experiments. *D*, quantification of cellular Aβ is shown. The data presented are the means ± S.D. of three independent experiments. *, $p < 0.05$; **, $p < 0.01$ *versus* LPL at 0 μg/ml. *E* and *F*, astrocytes were incubated with Aβ (500 nM) and LPL (2 μg/ml) at 37 °C for 0, 3, and 5 h. The cultured cells were then washed thoroughly in PBS three times, and the cells were collected. The amount of Aβ in the whole cell lysate was determined by Western blotting using 6E10 antibody. The level of actin demonstrated by Western blotting using the anti-β-actin antibody was used as the loading control. These data are representative of at least three independent experiments. *F*, quantification of cellular Aβ is shown. The data are the means ± S.D. of three independent experiments. *, $p < 0.001$ *versus* LPL (+) at 1 h.

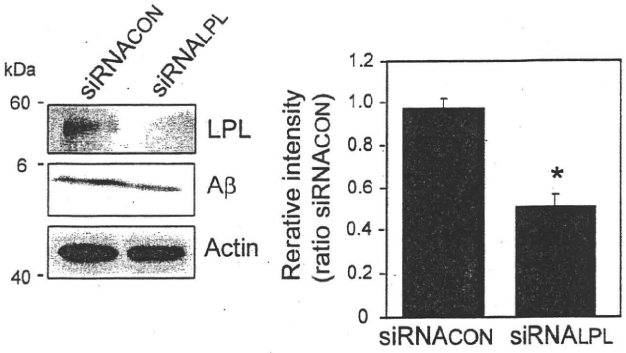

FIGURE 3. **Effect of LPL knockdown on cell-surface association of Aβ in cultured astrocytes.** Astrocytes were transfected with 10 nM siRNA specific for LPL (*siRNALPL*) and control siRNA (*siRNACON*). Forty-eight hours after transfection, cells were treated with Aβ42 (1 μM) at 4 °C for 3 h. The cells were washed in cold PBS three times, and the cells were harvested using a scraper. The level of Aβ42 on the cell surface was determined by Western blotting in a detergent extract of whole cells. The graph shows the levels of cell-surface-associated Aβ. The data are the means ± S.D. of three independent experiments. *, $p < 0.001$ *versus* control siRNA by unpaired Student's *t* test.

cells were treated with Aβ42 (1 μM) and then incubated at 4 °C for 3 h. As shown in Fig. 3, the cellular binding of Aβ42 to astrocytes was significantly decreased by LPL protein knockdown.

Degradation of Internalized Aβ in a Lysosomal Pathway in Astrocytes—Next, we examined the degradation of internalized Aβ. Mouse primary astrocytes were incubated with soluble Aβ42 and LPL at 37 °C for 5 h, washed in DMEM three times, and cultured at 37 °C for additional time (0, 3, 5, 12, and 24 h). Cells were then harvested, and the Aβ level in the cell lysate was analyzed by Western blotting. The strong signal representing internalized Aβ during the initial incubation for 5 h was detected in the cell lysate at the point of 0 min after washing (Fig. 4*A*). Three to five hours after washing, the level of Aβ remaining in the cell lysate partially disappeared (Fig. 4*A*). Twelve and twenty-four hours after washing, the internalized Aβ completely disappeared, indicating that the internalized Aβ was degraded in astrocytes in a time-dependent manner (Fig. 4*A*). To gain insight into the degradation pathway of the internalized Aβ, we investigated the localization of Aβ by immunocytochemical analysis. Mouse primary astrocytes were plated on poly-L-lysine-coated coverglasses and incubated with Aβ42 (500 nM) and LPL (2 μg/ml) at 37 °C for 5 h. In some experiments, cells were washed in DMEM three times and further incubated in serum-free DMEM for 3 h. Cells were then permeabilized and stained with an anti-Aβ antibody, 6E10, and an anti-LAMP2 antibody, whose staining signal is considered as a marker of late endosomes/lysosomes (21). We found that some portions of anti-Aβ antibody-positive signals were co-localized with staining signals reactive to the anti-LAMP2 antibody, showing that the internalized Aβ was trafficked into late endosomal/lysosomal compartments (Fig. 4*B*). To confirm the involvement of a lysosomal pathway in the degradation of LPL-mediated internalized Aβ, we determined the effect of chloroquine on the localization of Aβ internalized in an LPL-mediated manner. Chloroquine is a weak base and is taken up by cells, which results in the neutralization of acidic organelles such as lysosomes and impairment of their functions (22, 23). Chloroquine treatment at concentrations of 25 and 50 μg/ml prevented the degradation of internalized Aβ 12 h after washing out (Fig. 4*C*). We also tested inhibitors of neprilysin, an insulin-degrading enzyme, and cathepsin B, all of which are known to degrade Aβ. These inhibitors failed to suppress the degradation of internalized Aβ in astrocytes (data not shown). Thus, Aβ internalized in an LPL-mediated manner was degraded in a lysosomal pathway in astrocytes.

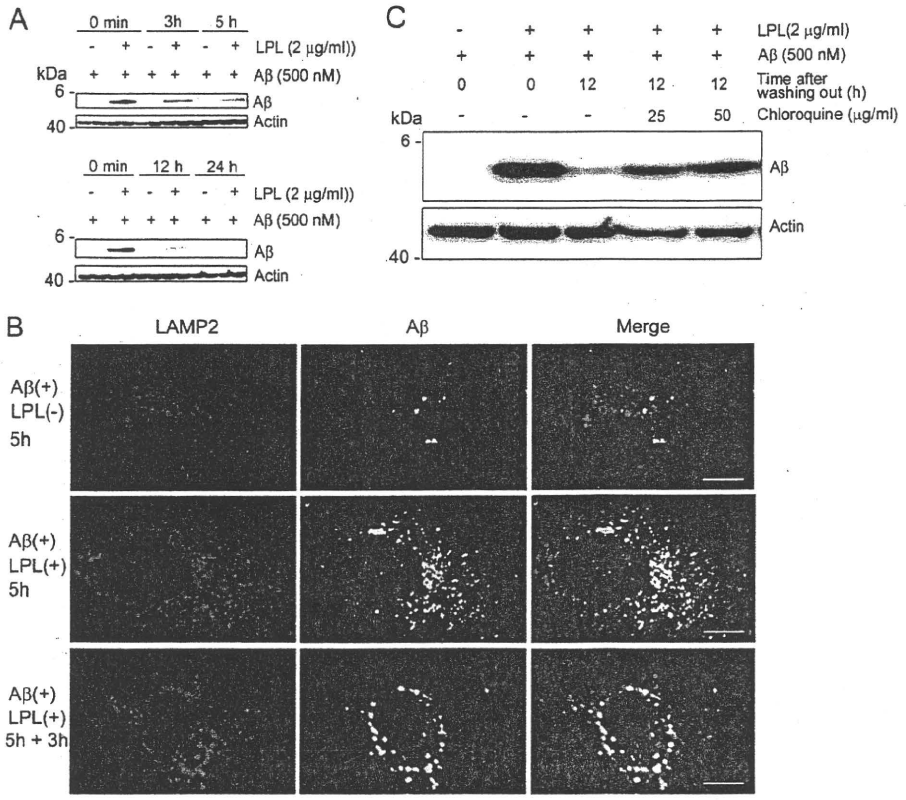

FIGURE 4. **Aβ is trafficked to late endosomal/lysosomal compartments and degraded after the LPL-mediated uptake.** *A*, mouse primary astrocytes were incubated with LPL (2 μg/ml) and Aβ (500 nM) at 37 °C for 5 h. Cells were washed in DMEM three times and then incubated in DMEM at 37 °C for 0, 3, 5, 12, and 24 h. The amount of Aβ remaining in the cells was determined by Western blotting using the anti-Aβ antibody, 6E10, in a detergent extract of whole cells. *B*, astrocytes were plated on poly-L-lysine-coated coverglasses and incubated with LPL (2 μg/ml) and Aβ (250 nM) at 37 °C for 5 h. Then, cells were permeabilized and double stained with an anti-LAMP2 antibody and 2C8. Bound antibodies were visualized with Cy3-conjugated (*red*) and FITC-conjugated (*green*) secondary antibodies for the anti-LAMP2 antibody and 6E10, respectively. Astrocytes incubated without Aβ did not show any anti-Aβ antibody-positive signals (not shown). *Scale bar*, 10 μm. *C*, astrocytes were incubated with LPL (2 μg/ml) and Aβ (500 nM) at 37 °C for 5 h. Cells were then washed in DMEM and cultured with or without chloroquine in DMEM at 37 °C for an additional 12 h. The level of Aβ in the detergent extract of whole cells was determined by Western blotting with 6E10. These are representative data of at least three independent experiments.

LPL Promotes Cellular Uptake of Aβ in a Heparan Sulfate- and Chondroitin Sulfate-dependent Manner—LPL has a high affinity with heparan sulfate (HS) and chondroitin sulfate (CS) (5, 24, 25). Therefore, we next investigated whether HS and CS are involved in the LPL-mediated cellular binding and cellular uptake of Aβ in astrocytes. Mouse primary astrocytes were pretreated with a mixture of heparinase II and heparinase III and/or chondroitinase ABC for 24 h at 37 °C, followed by incubation with Aβ42 and LPL at 4 °C for 3 h. There were no significant differences among the values in the absence of LPL (one-way ANOVA; $p = 0.0929$ for cell-surface-associated Aβ, $p = 0.4350$ for cellular Aβ). Pretreatment with heparinases or chondroitinase ABC partially decreased the level of LPL-mediated cellular binding of Aβ in astrocytes to 40 or 50% of that observed in the nontreated control, respectively (Fig. 5*A*). Interestingly, pretreatment with both heparinases and chondroitinase ABC decreased the level of LPL-mediated binding of Aβ to astrocytes to 20% of that observed in nontreated control (Fig. 5*A*). Next, we determined the effect of HS and/or CS on the LPL-mediated cellular uptake of Aβ. In conjunction with the effect of LPL on Aβ binding, heparinases and chondroitinase ABC decreased the level of LPL-mediated cellular uptake of Aβ in astrocytes to 30 and 50% of that observed in the nontreated control incubated with LPL, respectively (Fig. 5*B*). Pretreatment with both heparinases and chondroitinase ABC did not show an additive effect on the attenuation of LPL-promoted Aβ uptake (Fig. 5*B*). These findings indicate that HS and CS expressed in astrocytes are involved in the LPL-mediated association of Aβ with astrocytes and Aβ cellular uptake.

To further confirm the involvement of HS and CS in LPL-mediated Aβ uptake, we incubated astrocytes with various glycosaminoglycans. Heparin, which is a structural analog of HS, substantially suppressed the effect of LPL on Aβ uptake at a concentration of 3 μg/ml (Fig. 5*C*). The suppressive effect of heparin on LPL-mediated Aβ uptake was also observed in the presence of de-*N*-sulfated heparin, whereas either de-2-*O*-sulfated heparin or de-6-*O*-sulfated heparin had no effect on LPL-mediated Aβ uptake (Fig. 5*C*). None of these heparins interfered with the interaction between LPL and Aβ (Fig. 5*D*). In addition, 4-*O*-, 6-*O*-disulfated chondroitin sulfate (3 μg/ml) completely suppressed the promotive effect of LPL on Aβ uptake (Fig. 5*E*). 4-*O*-Sulfated chondroitin sulfate and 6-*O*-sulfated chondroitin sulfate moderately attenuated the function of LPL, whereas chondroitin (a nonsulfated form of chondroitin sulfate) and 2-*O*-, 6-*O*-disulfated chondroitin

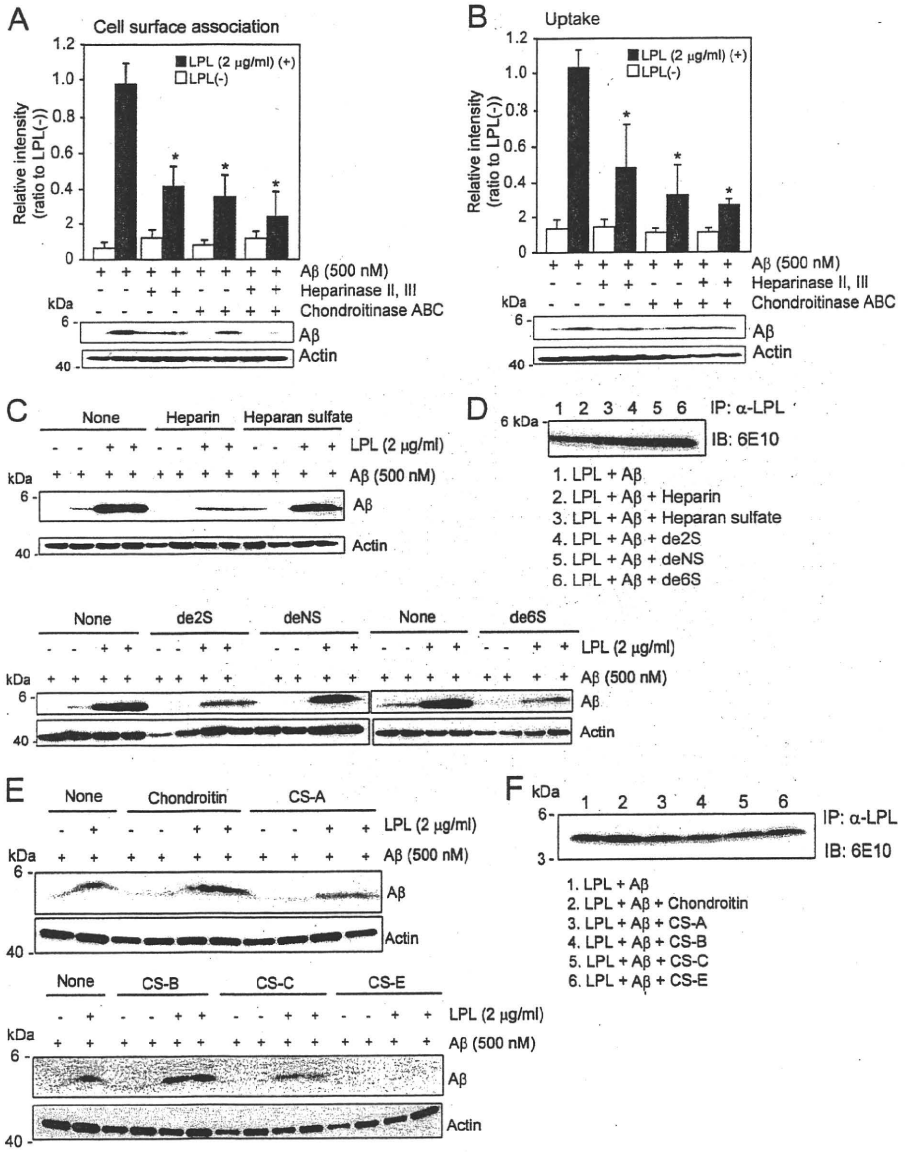

FIGURE 5. **LPL-mediated cellular binding and uptake of Aβ depends on heparan sulfate and chondroitin sulfate in astrocytes.** *A* and *B*, astrocytes from wild-type mice were pretreated with a mixture of heparinase II (0.03 μg/ml) and heparinase III (0.03 μg/ml), and/or chondroitinase ABC (0.03 μg/ml) at 37 °C for 24 h. After washing in DMEM three times, cells were incubated with LPL (2 μg/ml) and Aβ (500 nM) at 4 °C for 3 h (for cell surface association) (*A*) or 37 °C for 3 h (for uptake) (*B*). The level of Aβ in the detergent extract of whole cells was determined by Western blotting using 6E10. The quantitative assessment of cell-surface-associated Aβ (*A*) and cellular Aβ (*B*) in the present (closed bars) or absence (open bars) of LPL are shown. The data presented are the means ± S.D. of three independent experiments. * $p < 0.001$ *versus* levels of LPL (-). (*C*) Mouse primary astrocytes were incubated with Aβ (500 nM) or LPL (2 μg/ml) and Aβ (500 nM) in the presence or absence of heparin or chemically modified heparins at a concentration of 3 μg/ml at 37 °C for 5 h. The level of Aβ in the detergent extract of whole cells was determined using 6E10. (*D*) LPL (2 μg/ml) and Aβ (500 nM) were incubated in DMEM at 37 °C for 3 h in the presence or absence of heparin, heparan sulfate, or chemically modified heparins at a concentration of 3 μg/ml. Protein complexes in DMEM were immunoprecipitated (*IP*) with an anti-LPL antibody (α-LPL) and the Aβ recovered in the immunoprecipitates was analyzed by Western blotting using 6E10. These data are representative of at least three independent experiments. *de2S*, 2-*O*-desulfated heparin; *de6S*, 6-*O*-desulfated heparin; *deNS*, *N*-desulfated heparin. *E*, astrocytes were incubated with LPL (2 μg/ml) and Aβ (500 nM) in the presence or absence of chondroitin sulfates (chondroitin, chondroitin 4-sulfate (*CS-A*), 2-*O*-, 6-*O*-disulfated chondroitin sulfate (*CS-B*), 6-*O*-sulfated chondroitin sulfate (*CS-C*), and chondroitin 4,6-disulfate (*CS-E*)) at a concentration of 3 μg/ml at 37 °C for 5 h. The level of Aβ in a detergent extract of whole cells was determined by Western blotting using 6E10. *F*, LPL (2 μg/ml) and Aβ (500 nM) were incubated in DMEM at 37 °C for 3 h in the presence or absence of chondroitin sulfates at a concentration of 3 μg/ml. Protein complexes were immunoprecipitated with the anti-LPL antibody (α-LPL), and the Aβ recovered in the immunoprecipitates was analyzed by Western blotting using 6E10. The data are representative of at least three independent experiments. *IB*, immunoblot.

sulfate (also known as dermatan sulfate) did not (Fig. 5*E*). None of these CS interfered with the interaction between LPL and Aβ *in vitro* (Fig. 5*F*).

ApoE Is Dispensable for LPL-mediated Cellular Uptake of Aβ in Astrocytes—Because ApoE is reported to be involved in the metabolism of Aβ, including its aggregation and clearance (26), we analyzed the effects of ApoE on the LPL-mediated cellular uptake of Aβ in astrocytes. We collected culture media of primary astrocytes prepared from ApoE-KO mice and C57BL/6 (WT) mice. The astrocyte cultures prepared from wild-type mouse cortices were incubated in conditioned media in the presence of Aβ42 and LPL. As shown in Fig. 6A, Aβ